

Gunshot acoustic event identification and shooter localization in a WSN of asynchronous multichannel acoustic ground sensors

S. Astapov¹  · J. Berdnikova² ·
J. Ehala¹ · J. Kaugerand¹ · J.-S. Preden¹

Received: 17 February 2016 / Revised: 20 December 2016 / Accepted: 15 February 2017
© Springer Science+Business Media New York 2017

Abstract Gunshot acoustic localization for military and civilian security systems has long been an important topic of research. In recent years the development of Wireless Sensor Network (WSN) systems of independent Unmanned Ground Sensors (UGS) performing distributed cooperative localization has grown in popularity. This paper considers a shooter localization approach based on gunshot Shockwave (SW) and Muzzle Blast (MB) event time and Direction of Arrival (DOA) information. The approach accounts for acoustic events Not-of-Interest (NOI), such as target hit noise, reflections and background noise. UGS perform gunshot acoustic event detection and DOA estimation independently; the information regarding every detected shot instance is sent through the WSN to the fusion node, which performs event identification and calculates the shooter's position. The paper presents a solution to identifying SW and MB among NOI events at the stage of information fusion. The considered approach treats the information gathered from different UGS separately, and thus does not require precise synchronization between the UGS. For DOA estimation, an

This research was supported by the European Defense Agency project IN4STARS and the Estonian IT Academy program.

✉ S. Astapov
sergei.astapov@ttu.ee

J. Berdnikova
julia.berdnikova@ttu.ee

J. Ehala
johannes.ehala@ttu.ee

J. Kaugerand
jaanus.kaugerand@ttu.ee

J.-S. Preden
jurgo.preden@ttu.ee

¹ Laboratory for Proactive Technologies, Department of Software Science, Tallinn University of Technology, Ehitajate tee 5, 19086 Tallinn, Estonia

² Thomas Johann Seebeck Department of Electronics, Tallinn University of Technology, Ehitajate tee 5, 19086 Tallinn, Estonia

algorithm designed for circular microphone arrays is proposed and compared with the SRP-PHAT localization algorithm. It is shown to provide adequate DOA estimates, while being more computationally effective. The proposed shooter localization approach is tested on real signals, acquired during three live shooting experiments. It is shown to succeed in localizing the shooter's position with a mean accuracy of 0.87 m for 30 shots at the range of 35 m, and just above 7 m for 37 shots at the range of 100 m.

Keywords Shooter acoustic localization · Circular microphone arrays · DOA estimation · SRP-PHAT · Wireless Sensor Networks

1 Introduction

Active development of shooter acoustic localization systems has continued for more than three decades. Numerous different gunshot detection and direction estimation systems are currently available for military applications of sniper and covert enemy force positioning, and are also used in law enforcement for gun violence reduction and forensics (Aguilar 2013). The devices currently available are generally standalone systems, composed of a single microphone array, e.g., the vehicle-mountable Boomerang system (Mazurek et al. 2005). Individual gunshot detectors, developed for military and law enforcement personnel (George and Kaplan 2011; Sallai et al. 2013; George et al. 2014), consist of compact shoulder-carried, helmet or uniform mounted sensors. Such individual systems increase local situation awareness, however, for large area coverage a different approach is required.

Modern Military Intelligence, Surveillance and Reconnaissance (ISR) systems apply distributed Unmanned Ground Sensors (UGS) interconnected through a Wireless Sensor Network (WSN) for large area coverage. UGS perform local situation assessment, and through data fusion a global assessment over the whole monitored area is made. A distributed system configuration expands UGS collective Field of View (FOV) and thus is well suited for shooter localization. The state of the art in this area suggests either synchronous (Sallai et al. 2011), or asynchronous (Damarla et al. 2010) gunshot acoustic event detection and subsequent shooter localization based on UGS collective information. The majority of the proposed approaches are based on the supersonic bullet's shockwave (SW) and muzzle blast (MB) analysis (Millet and Baligand 2006). Most methods employ single-sensor UGS which identify the gunshot events and estimate the shot geometry under different initial assumptions, e.g., the known caliber of the fired projectile in Sallai et al. (2011), or a certain ballistic shockwave acoustic model in Aguilar et al. (2007). However, initial assumption inconsistency and the presence of acoustic events Not-of-Interest (NOI) may significantly reduce localization accuracy (Ash et al. 2010). (By NOI events we denote residual gunshot acoustic events and various noise produced by other sources.)

Employing multichannel smart sensors for gunshot localization allows to additionally estimate the Direction of Arrival (DOA) of gunshot event acoustic waves. Knowing the DOA aids in acoustic event identification and allows to reduce the number of initial assumptions, which, in turn, makes the localization process more robust. In this paper we propose a method of shooter localization based on gunshot event DOA and Time Difference of Arrival (TDOA) information. The method is intended for operation in a WSN which consists of interconnected UGS, equipped with sensor arrays, and information fusion nodes. Each UGS independently performs gunshot acoustic event detection, computes the DOA and fixates event occurrence time in its own local time. The fusion node gathers DOA and time information from all the UGS which it governs, performs identification of SW and MB among NOI events, calculates

the TDOA between SW and MB, and estimates the shooter position based on the UGS known positions. The distribution of computational tasks among the UGS and fusion nodes reduces the risk of any network component being overloaded, and the use of several fusion nodes eliminates the single point of failure and bottleneck effects. The TDOA are calculated per each UGS and no cross-UGS delays are used, thus node synchronization is not required (however, node clock divergence still needs to be roughly estimated for the fusion node to be able to distinguish between shot instances). An asynchronous approach is explicitly targeted due to the fact that long-lasting precise node synchronization cannot be guaranteed in WSN, especially in ones adopting the dynamic ad-hoc topology. For DOA estimation we apply a reduced computational cost approach presented by us in [Astapov et al. \(2015a\)](#), and a well known, effective, but computationally expensive localization algorithm of Steered Response Power (SRP-PHAT) for comparison.

Circular microphone arrays were chosen for the UGS implementation to allow for a 360° horizontal Field of View (FOV). Two prototype versions were created: the first one employs six condenser microphones and an exterior Data Acquisition Device (DAQ); the second one employs six MicroElectroMechanical Systems (MEMS) microphones and a BeagleBone Black as a DAQ and processing unit. The proposed method is tested on signals acquired during three live shooting experiments. The first experiment was performed at a small outdoor shooting range with a shooter-target distance of 35 m. The signals were acquired by four UGS of prototype 1. The second and third experiments were performed at a larger outdoor shooting range with a shooter-target distance of 100 m. The signals were acquired by six UGS of prototype 2. The experimental results indicate the feasibility of the proposed localization method in terms of gunshot event detection, NOI event elimination and shooter position estimation.

The remainder of the paper is structured as follows. Section 2 introduces the applied gunshot geometry model. Section 3 discusses problems situated with shooter acoustic localization, while examining several gunshot scenarios and localization approaches. Section 4 handles the proposed shooter localization method, reviewing the gunshot acoustic event detection, DOA estimation and information fusion procedures. Section 5 presents the UGS prototypes and experimental results. Section 6 is devoted to the discussion and thoughts on future developments. Finally, Sect. 7 concludes the paper.

2 Gunshot acoustic components

For our shooter localization approach we adopt a planar gunshot acoustic event geometry model (i.e., the sensor and the trajectory of the traveling bullet are situated in the horizontal plane). Figure 1 portrays the acoustic events produced by a gunshot at point Z , as observed

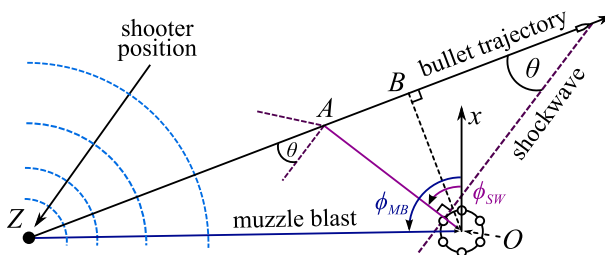


Fig. 1 Gunshot acoustic event geometry in the horizontal plane

at point O . For simplicity purposes we assume straight bullet trajectory, not accounting for effects considered in exterior ballistics (Carlucci and Jacobson 2010). A gunshot is characterized by the shockwave, produced by a supersonic projectile, and the muzzle blast of the fired weapon. SW produces a conical wavefront at an angle θ to the bullet's trajectory. The angle θ depends on the speed of sound c in air and the bullet velocity v :

$$\theta = \sin^{-1} \frac{c}{v}. \tag{1}$$

The waves of MB, on the other hand, propagate spherically at speed c in all directions.

The initial bullet velocity is equal to the muzzle velocity v_0 (i.e., the velocity at which the bullet leaves the muzzle of a gun), which depends on the bullet caliber and cartridge type and can be approximated for different firearm types (Carlucci and Jacobson 2010). Bullet velocity v decreases with flight distance due to air friction. It can be expressed as a function of traveled distance d_f as

$$v(d_f) = \left(v_0^\eta - 2\eta C_b^{-1} d_f \right)^{1/\eta}, \tag{2}$$

where, C_b is a ballistic constant, which depends on the bullet's type, and η is the exponent value, usually set at 0.5. We assume function (2) to be unknown and rather estimate the bullet velocity using the procedure described in Sect. 4.3.3. For small firearms (e.g., rifles) the decrease in the $v(d_f)$ curve can be considered linear and ultimately insignificant for the travel distance of 100–200 m (Carlucci and Jacobson 2010). Thus, for the rest of the paper we denote the bullet velocity as a range-invariant parameter v . The speed of sound in air c , on the other hand, depends on the ambient temperature. For an open environment it is calculated as

$$c = 331.45 \sqrt{1 + t^\circ / 273}, \tag{3}$$

where, t° is the temperature in degrees Celsius.

At line-of-sight, the sensor at point O detects MB at the time

$$t_{MB} = t_{shot} + \frac{d_{Z,O}}{c}, \tag{4}$$

where, t_{shot} is the time of shot, and $d_{Z,O} = \|Z - O\|$ is the Euclidean distance between points Z and O . Acoustic waves of SW originate from the bullet itself and not from the muzzle. SW travels outwards from the bullet's trajectory and is approximated as a planar wavefront in the horizontal plane. As the bullet has reached point A at speed v , the SW wavefront propagates from point A at speed c and reaches point O at the time

$$t_{SW} = t_{shot} + \frac{d_{Z,A}}{v} + \frac{d_{A,O}}{c}. \tag{5}$$

Point A here is such a point on the bullet's trajectory, from where SW will travel directly to point O at an angle θ relative to the bullet's trajectory (see Fig. 1).

The TDOA between SW and MB acoustic events can then be expressed as

$$\Delta t = t_{MB} - t_{SW} = \frac{d_{Z,O}}{c} - \frac{d_{Z,A}}{v} - \frac{d_{A,O}}{c}. \tag{6}$$

The distance from the sensor at point O to the bullet's trajectory ($d_{O,B}$ in Fig. 1) is called the miss distance. Whether Δt is positive depends on the bullet's velocity and the miss distance. In case of a shot fired from a rifle (average bullet velocity near or greater than mach 2) in the sensor's direction with the miss distance small enough, Δt is expected to be positive, as SW will most likely reach the sensor before MB.

The DOA of MB and SW for the sensor at point O are defined in the horizontal plane as azimuth values ϕ_{MB} , ϕ_{SW} , relative to the sensor's local coordinate system (x -axis in Fig. 1). Here the azimuth ϕ_{SW} is the angle of incidence of a wavefront traveling from point A , and ϕ_{MB} is the angle of incidence of a wavefront traveling from point Z .

3 Problem statement

Knowing t_{SW} and t_{MB} , gunshot acoustic localization may be performed by estimating the angle θ and the miss distance. Angle θ may be estimated by applying a shockwave acoustic model to the duration of the SW transient (Aguilar et al. 2007), or calculated under known bullet caliber assumption (Sallai et al. 2011). Then, using multiple measurements of t_{SW} and t_{MB} from K synchronous single-sensor UGS, the miss distances can be approximated and point Z located via a search procedure proposed by Sallai et al. (2011). UGS synchronization plays a crucial role in such approaches and heavily influences the bound parameters of the bounded search procedure, as well as the overall localization accuracy, as discussed by Lindgren et al. (2009). Alternatively, using multiple measurements from K asynchronous single-sensor UGS and assuming θ to be known, it is possible to iteratively estimate MB DOA, miss distances, the bullet's trajectory and, consequently, point Z via a multistage optimization procedure proposed by Damarla et al. (2010). If UGS clocks are sufficiently synchronized, a mutual reference moment t_{shot} can be established for all UGS via (5), and Z can be estimated by multilateration, using time delays t_{MB} from (4). Multilateration and its application to shooter localization is discussed further in the "Appendix".

Unfortunately, if gunshot events include NOI events, such as reflections and target hit (TH) noise, MB cannot be unambiguously selected from numerous events following SW. Consider, for example, Fig. 2, which presents six fundamental gunshot scenarios. Scenarios I–III do not contain NOI events and are most commonly considered in the majority of state of the art approaches. In Scenarios I and II the bullet either passes through or beside the UGS cluster, and no TH is detected. The localization is then performed using pure SW readings (arrows pointing from one or both sides towards the bullet's trajectory) and MB readings (arrows pointing towards the shooter's position). Scenario III assumes that only MB are detected. This makes it a trivial localization problem which can be solved using conventional localization methods, e.g., multilateration. Scenarios IV–VI, on the other hand, assume the presence of NOI events and the masking effect. Here either SW or MB may be corrupted or masked by TH (Scenario V), or either SW or MB may be corrupted or masked by each other (Scenarios IV and VI). Furthermore, NOI such as reflections and background noise may be present for all scenarios and must be accounted for accordingly. NOI events can be eliminated by identifying MB and SW by their acoustic properties (Libal and Spyra 2014) or applying statistical assignment (Osborne et al. 2014), however, these do not solve the masking problem.

The shooter localization algorithm presented in this paper assumes Scenario V of Fig. 2, where the UGS form a look-out perimeter around the potential target, that is very likely to be hit inside or near the UGS cluster. Scenario V implies that either SW or MB may be corrupted or masked by TH, and UGS situated behind the target may not detect SW altogether. As Scenario I is a special case of Scenario V (the bullet passes through the cluster and no TH is detected), the localization rules intended for Scenario V will also be applicable for Scenario I.

The paper also considers several acoustic event detection problems situated with varying shot range and influence of NOI events. At a sufficient shot range the TDOA between SW and

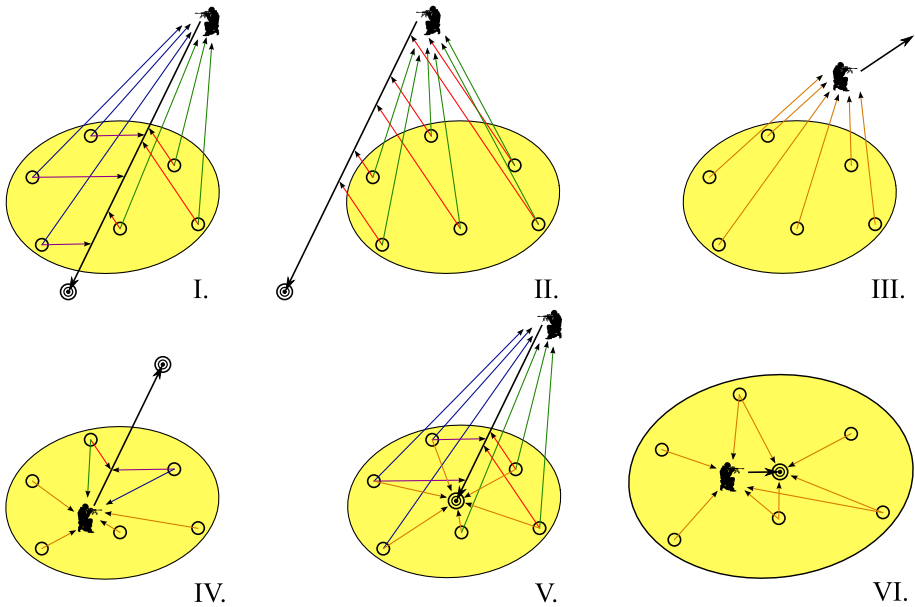


Fig. 2 Six fundamental gunshot scenarios: the bullet passes through the UGS cluster (I); the bullet passes beside the UGS cluster (II); a shot is fired away from the UGS cluster (III); a shot is fired from inside the UGS cluster (IV); the bullet hits the target in the vicinity of the UGS cluster (V); a shot is fired and the bullet reaches its target inside the UGS cluster (VI)

MB acoustic transients makes the events well distinguishable (Borzino et al. 2014). In one of our experiments we study a short range case, where event separation is not straightforward due to short TDOA. In our detection method we account for all gunshot acoustic events, as the MB transient is not guaranteed to strictly follow the SW transient.

4 Proposed approach to shooter localization

The proposed approach is intended for application in WSN with a dynamic ad-hoc topology. This implies node synchronization complications and a varying number of active nodes at any given time. Thus, we focus on an asynchronous, size-invariant solution. The WSN consists of UGS, equipped with acoustic sensor arrays, and one or several information fusion nodes. The approach consists of the following steps:

1. Each UGS detects a gunshot, separates its acoustic events, marks the time and computes a DOA value per each event.
2. Per each detected shot, each UGS sends an information packet to the fusion node, containing its position, steering angle and acoustic event parameters $\{\mathbf{x}, \beta, \mathbf{t}, \Phi\}$.
3. The fusion node performs event identification and shooter localization based on the information provided by active UGS.

The packet of UGS $k = 1, \dots, K$ contains: UGS coordinates $\mathbf{x}_k = (x_k, y_k)$; UGS steering angle β_k ; gunshot event times $\mathbf{t}_k = [t_1, \dots, t_{E_k}]$; event DOA $\Phi_k = [\phi_1, \dots, \phi_{E_k}]$, where E_k is the number of detected events of k -th UGS. As each UGS operates in its own coordinate system, the steering angle β_k is used to specify UGS local coordinate system steering from

a global zero-rotation angle (which is defined by Earth's magnetic north). While receiving packets from UGS, the fusion node maintains a validity interval, beginning at the moment of arrival of the first packet. This way the expired packets, or the ones corresponding to another shot are dealt with separately.

For the sensor configuration we choose Uniform Circular Arrays (UCA) because they provide full horizontal FOV with a simple geometry. Each array consists of $M = 6$ microphones with an angle between two successive microphones, relative to the array center O , of

$$\alpha = \angle m_i O m_{i+1} = \frac{2\pi}{M}, \quad (1 \leq i < M). \quad (7)$$

The arrays are designed to be compact, since the application field requires UGS to be covert, if hidden in the monitored environment. For the UCA experimental prototypes we use circular shells with a radius of $r = 7.5$ cm (prototype 1) and $r = 10$ cm (prototype 2).

4.1 Gunshot acoustic event detection and separation

Gunshot acoustic event detection for a general case (i.e., comprising of all scenarios of Fig. 2) is an intricate task. Amplitude-based methods are well suitable in case of Scenarios IV and VI, where both SW and MB are detected inside the UGS cluster as high-energy transients and are, therefore, distinguishable from background noise. The same holds for Scenarios I–III and V if the range is short enough for MB to be detected. Otherwise, MB can have an insufficiently high amplitude to be detected, or it can be masked by background noise. Another approach lies in identifying SW and MB by the shape of their acoustic signals. [Aguilar et al. \(2007\)](#) examine the N-shaped pattern of SW, and [Libal and Spyra \(2014\)](#) try to distinguish SW and MB from reflections by applying classification. This may work well for Scenarios I–III, where no TH or overlapping events occur and the task lies in eliminating reflections. For Scenarios IV–VI and, in our case specifically, Scenario V these methods are not guaranteed to perform well.

Shooter distance plays an important role in acoustic event separation as well. In case of a significantly short distance, acoustic event separation poses a challenge due to an extremely short TDOA between SW and MB ([Freire and Apolinario 2011](#)). Figure 3 presents an example of a normalized gunshot signal acquired 16.2 m away from the shooter. Here the TDOA between SW (at 4 ms) and MB (at 11 ms) is only 7 ms. Figure 5, on the other hand, portrays a normalized gunshot signal acquired 97.5 m away from the shooter. Here the TDOA between SW (at 25 ms) and MB (at 150 ms) is already 125 ms, which is twice as long as the whole gunshot signal of Fig. 3. If the detection algorithm treats the closely spaced events as a single event, MB may be lost in the SW transient. On the other hand, analyzing every closely spaced signal peak will waste computational resources and produce a large number of unwanted results.

Another problem lies in separating gunshot instances in case of burst-mode and automatic fire at close ranges. Consider Fig. 3, where the TDOA between SW and MB is 7 ms with post-blast events (TH and reflections) starting to occur at the 40th millisecond. Neglecting these post-blast events may seriously harm the detection process in case of burst-mode fire. For example, an AK-47 in burst mode can fire 600 rounds per minute and an M-4 fires at 950 rpm, which constitutes approximately 1 bullet every 100 ms and 63.2 ms, respectively. In this case consecutive SW and MB may be mistaken for post-blast events, and vice versa for a single shot case.

In our approach to acoustic event detection and separation we consider both short (20–40 m) and medium (100–200 m) shot distances. We establish all acoustic events by

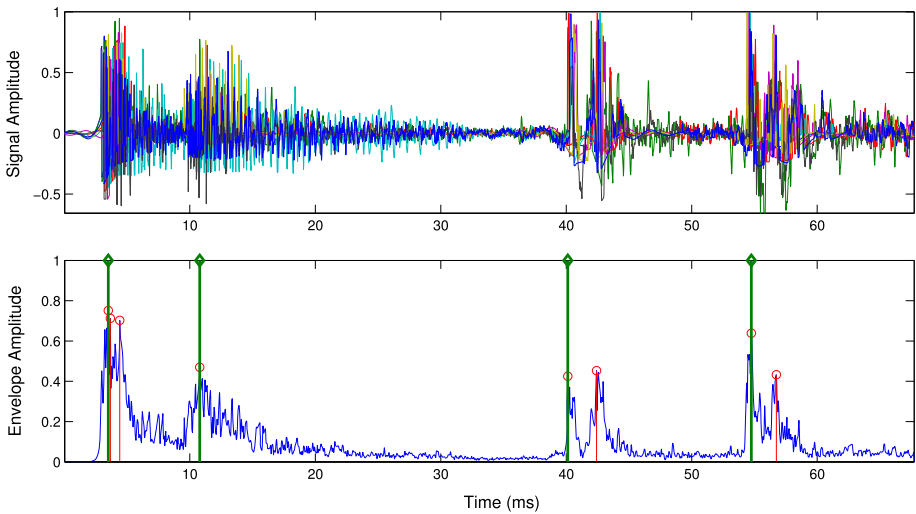


Fig. 3 Gunshot acoustic components acquired by UGS S_3 , Experiment 1, at 48 kS/s (*top*). Collective envelope and times of detected events (*bottom*). *Red stems* results of peak detection; *green stems* event establishing peaks

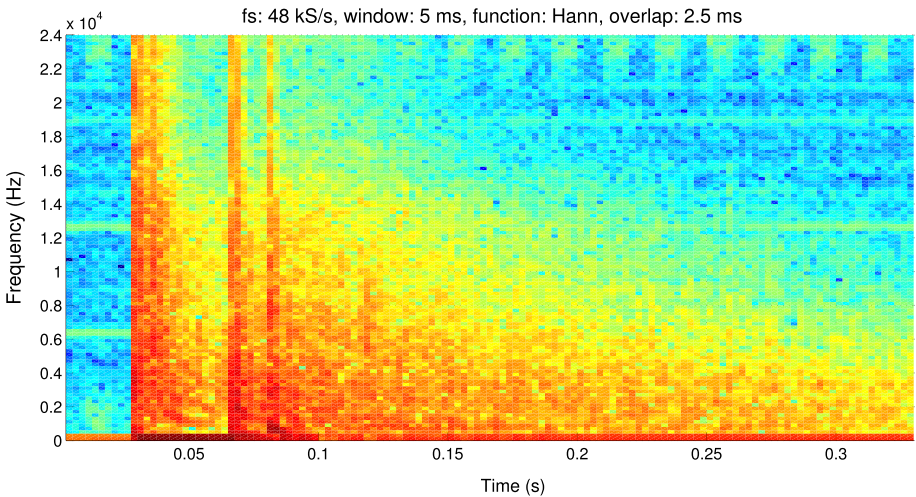


Fig. 4 Spectrogram of the gunshot signal presented in Fig. 3. Acoustic components presented in Fig. 3 are located at approximately 30–95 ms.

the following procedure. First, a collective envelope is computed using the signals from all microphones. At sampling time n , the envelope of samples $x_1[n], \dots, x_M[n]$ is

$$s_{\text{env}}[n] = \max(|x_1[n]|, \dots, |x_M[n]|). \tag{8}$$

Event detection is performed on the differential collective envelope

$$\Delta s_{\text{env}}[n] = s_{\text{env}}[n] - s_{\text{env}}[n - 1]. \tag{9}$$

The differential envelope $\Delta s_{\text{env}}[n]$ is passed through peak detection, and peaks within an interval of $t_W/2$ seconds, where t_W is the predefined length of event window, are grouped

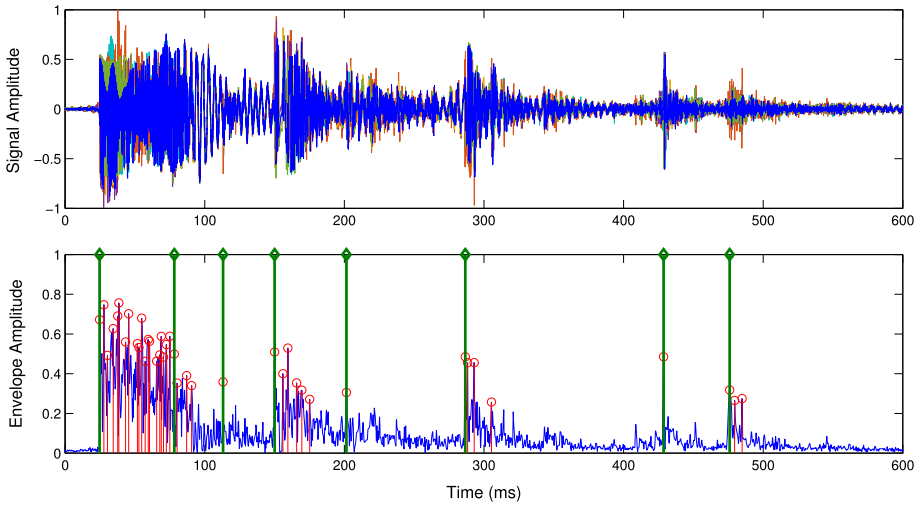


Fig. 5 Gunshot acoustic components acquired by UGS S_1 , Experiment 3, shooter position 1, at 20 kS/s (top). Collective envelope and times of detected events (bottom). Red stems results of peak detection; green stems event establishing peaks

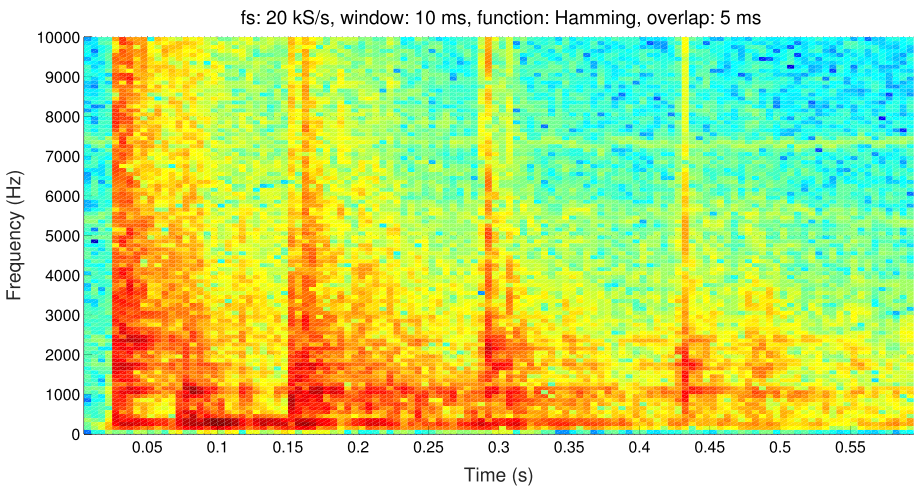


Fig. 6 Spectrogram of the gunshot signal presented in Fig. 5

together and one (the first) peak per event is chosen. An example of separation of four events is presented in Fig. 3 (lower) and of eight events—in Fig. 5 (lower). One frame of duration t_W is retrieved from the multichannel signal buffer per each event peak such, that event beginning is included in the frame and adjacent events are strictly separated. This means that if the events do not overlap, the event is windowed from the beginning of its signal’s envelope rise for the duration t_W ; if the events do overlap (event establishing peaks are approximately $t_W/2$ seconds apart), the first event is windowed leftward from the beginning of the second event, and the second event is windowed rightward from it’s beginning.

Event identification is performed during the information fusion stage. As NOI events can also be transient in nature, they are hard to identify during event detection. Frequency analysis does not offer a straightforward solution either, as NOI events such as TH possess highly uniform spectral densities as well as SW and MB (see Figs. 4, 6). Figure 5 also portrays event overlapping at 25–110 ms. Here SW is overlapped with its own ground reflection, which results in two additional peaks being detected before MB. In this situation the identification of SW by its shape and duration will likely produce inaccurate results.

4.2 Direction of arrival estimation

At the time of shot detection, k -th UGS produces E_k multichannel signal frames of length $N = f_s t_W$, where f_s is the sampling frequency. A separate DOA estimate is then computed per each frame by applying SRP-PHAT (for reference) and our proposed lightweight method (Astapov et al. 2015a).

4.2.1 SRP-PHAT

Steered Response Power with Phase Transform is one of the most effective acoustic DOA estimation methods, proposed by DiBiase (2000). The SRP $P(\mathbf{a})$ is a real-valued functional of a spatial vector \mathbf{a} , the maxima of which indicate the direction to the sound source. $P(\mathbf{a})$ is computed as the cumulative Generalized Cross-Correlation with Phase Transform (GCC-PHAT) across all pairs of sensors at the theoretical time delays, associated with the chosen direction. Consider a pair of signals $x_k(t), x_l(t)$ of an array consisting of M microphones. The time instances of sound arrival from a point $a \in \mathbf{a}$ for the two microphones are $\tau(a, k)$ and $\tau(a, l)$, respectively. Hence the time delay between the signals is $\tau_{kl}(a) = \tau(a, k) - \tau(a, l)$. The SRP-PHAT for all pairs of signals is then defined as

$$P(a) = \sum_{k=1}^M \sum_{l=k+1}^M \int_{-\infty}^{\infty} \Psi_{kl} X_k(\omega) X_l^*(\omega) e^{j\omega\tau_{kl}(a)} d\omega, \tag{10}$$

where $X_i(\omega)$ is the spectrum (i.e., the Fourier Transform) of signal $x_i(t)$, $X_i^*(\omega)$ is the conjugate of that spectrum and Ψ_{kl} is the PHAT weight, defined as

$$\Psi_{kl} = (|X_k(\omega) X_l^*(\omega)|)^{-1}. \tag{11}$$

In a general case the spatial vector \mathbf{a} partitions the FOV into a planar or volumetric discrete spatial grid. An SRP value is then computed for every point of that spatial vector. This approach requires a significant amount of computational resources and is ultimately unneeded in our planar case. To reduce the number of SRP-PHAT computations we divide the horizontal plane into n_h possible azimuth angles. A single angle increment is calculated, similarly to (7), as $\phi_h = \frac{2\pi}{n_h}$. The evaluation points are chosen in the planar FOV along a circle with a radius r_{FOV} . The SRP-PHAT evaluation is performed over the entire circumference $[0, 2\pi)$ for the points $a_{h,i} = (x_{h,i}, y_{h,i})$:

$$\begin{aligned} x_{h,i} &= r_{FOV} \cos(i\phi_h), \quad (0 \leq i < n_h), \\ y_{h,i} &= r_{FOV} \sin(i\phi_h), \quad (0 \leq i < n_h). \end{aligned} \tag{12}$$

The azimuth is estimated in the direction of elevated SRP values $P(\mathbf{a}_h)$. For a single source case the final azimuth is equal to

$$\phi = \arg \max (P(\mathbf{a}_h)) \cdot \phi_h. \tag{13}$$

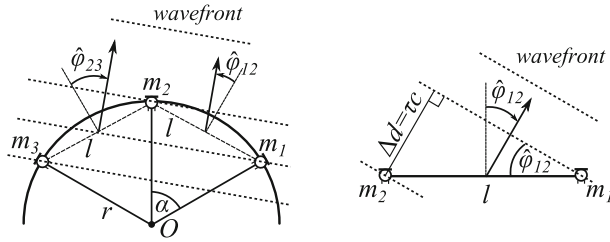


Fig. 7 Azimuth estimation in the far field for consecutive microphone pairs of the circular array (left). Geometry of a single microphone pair (right)

4.2.2 Optimized DOA estimation algorithm

Even with a reduced functional, SRP-PHAT still requires significant resources and processing time, because it performs cross-correlation between all pairs of microphones and for all specified directions. We focus on reducing the number of microphone pairs for cross-correlation and the number of discrete directions per each pair (Astapov et al. 2015a).

Our proposed method takes a directional DOA estimation approach. According to our design the microphones are embedded in a solid circular shell; therefore the DOA opposite to the common direction of any given microphone pair are not considered for analysis. The pairs of microphones for azimuth estimation are chosen such, that their inter-sensor angle is less than $\frac{\pi}{2}$: $\alpha_{ij} = \angle m_i O m_j < \frac{\pi}{2}$. The set of these pairs is

$$A = \left\{ (m_i, m_j) \subseteq S_2^M \mid \alpha_{ij} < \frac{\pi}{2} \right\}, \tag{14}$$

where S_2^M is the set of all combinations of microphone pairs, $|S_2^M| = \binom{M}{2}$. A separate azimuth estimate $\hat{\phi}_{ij}$ is made under the far field assumption for every pair of microphones $(m_i, m_j) \subseteq A$. For any pair (m_i, m_j) of consecutive microphones (see Fig. 7), the azimuth estimate is obtained by

$$\hat{\phi}_{ij} = \sin^{-1} \left(\frac{\tau_{ij} \cdot c}{l} \right) = \sin^{-1} \left(\frac{\Delta n_{ij} / f_s \cdot c}{l} \right), \tag{15}$$

where l is the distance between two consecutive microphones, calculated as

$$l = 2r \sin \left(\frac{\alpha}{2} \right) = 2r \sin \left(\frac{\pi}{M} \right), \tag{16}$$

and τ_{ij} is the TDOA of the wavefront to microphones m_i and m_j . For non-consecutive microphones, l is calculated by substituting α in (16) with its multiple. The TDOA is always limited to $\tau \in [-\tau_{\max}, \tau_{\max}]$, where $\tau_{\max} = l/c$ is the delay of sound traveling directly from one microphone to the other (i.e., at $\pm \frac{\pi}{2}$). In (15), τ_{ij} is also represented in terms of delay in samples Δn_{ij} and the sampling frequency f_s . To estimate Δn_{ij} we apply cross-correlation to the pair of signals:

$$R_{ij}(\Delta n) = \sum_{n=0}^{N-1} x_{m_i}[n] \cdot x_{m_j}[n - \Delta n], \quad (i < j), \tag{17}$$

where N is the length of the signals in samples. The maximum of the cross-correlation then defines the TDOA: $\Delta n_{ij} = \arg \max (R_{ij}(\Delta n))$. The quality of the estimate $\hat{\phi}_{ij}$ is measured

as cross-correlation peak distinctness from its mean level:

$$q_{ij} = \max (R_{ij} (\Delta n)) - \text{mean} (R_{ij} (\Delta n)). \tag{18}$$

Each estimate $\hat{\varphi}_{ij}$ is made for the middle point of the inter-microphone distance and takes the values of $\hat{\varphi}_{ij} \in [-\frac{\pi}{2}, \frac{\pi}{2}]$, negative if the source is situated to the left, positive—if the source is situated to the right, and zero—if it is in front of the microphone pair. Thus individual $\hat{\varphi}_{ij}$ are adjusted to the array’s common angle coordinates: $\hat{\varphi}_{ij}^* = \hat{\varphi}_{ij} + ((i - 1)\alpha + (j - 1)\alpha) / 2$. After that coherent directions are found among the estimates. This is done by applying a partitioning procedure, similar to the one we presented in Astapov et al. (2013). It performs the task of clustering the $\hat{\varphi}_{ij}^*$ estimates such, that the coherent estimates must lie within sectors with a central angle of no more than φ_{\max} . For example, if $\varphi_{\max} = \frac{\pi}{6}$, then each cluster’s coherent estimates must lie no more than $[-\frac{\pi}{12}, \frac{\pi}{12}]$ from the cluster’s centroid.

The resulting clusters $\Phi_p, p = 1, \dots, P$, where P is the number of clusters, each contain n_p estimates $\hat{\varphi}_k, k = [1, n_p]$, and the associated quality q_k . The clusters are evaluated in order to find the largest cluster, containing estimates of best quality (Astapov et al. 2015a). Algorithm 1 handles the final azimuth calculation for the single source case. The real-valued parameter $\sigma = (0, 1)$ is the threshold of tolerance and the integer parameter n_{\min} is the lower bound for the largest cluster size. The final azimuth estimate ϕ cannot be made if there are insufficient coherent estimates, or if they are of low quality.

Algorithm 1 Final azimuth ϕ estimation for a single source

```

Require:  $\Phi_p, q_k$  of every  $\hat{\varphi}_k \in \Phi_p, p = 1, \dots, P$ 
1: get largest cluster size  $|\Phi|_{\max}$ , maximum quality  $q_{\max}$ 
2: if  $|\Phi|_{\max} = n_{\min}$  or  $q_{\max} < \text{allowed}$  then
3:   return  $\phi \leftarrow \emptyset$  ▷ initial criteria not met
4: else if  $\Phi_p$  of size  $|\Phi|_{\max}$  contains  $\hat{\varphi}_k$  with  $q_{\max}$  then
5:   return  $\phi \leftarrow \sum_{k=1}^{n_p} q_k \hat{\varphi}_k / \sum_{k=1}^{n_p} q_k$  ▷ weighted mean
6: else
7:   for  $i = |\Phi|_{\max} - 1$  to  $i > n_{\min}$  do ▷ search in smaller  $\Phi_p, n_p > n_{\min}$ 
8:     if  $\exists q_k \geq \sigma \cdot q_{\max}$  for any  $\hat{\varphi}_k \in \Phi_p, |\Phi_p| = i$  then
9:       return  $\phi \leftarrow \sum_{k=1}^i q_k \hat{\varphi}_k / \sum_{k=1}^i q_k$ 
10:    end if
11:  end for
12:  return  $\phi \leftarrow \emptyset$  ▷ estimates of sufficient quality not found
13: end if

```

An example of final azimuth ϕ estimation based on the intermediate estimates $\hat{\varphi}_{ij}^*$ is presented in Fig. 8. Coherent directions are first established by applying the partitioning procedure with the φ_{\max} parameter. The resulting clusters Φ_1, Φ_2 and Φ_3 contain only one azimuth value because they do not lie within a sector with the central angle less than φ_{\max} , which means that the coherency condition is not met for these azimuth values. The clusters Φ_4 – Φ_6 , on the other hand, do contain coherent estimates. Then, according to Algorithm 1, the largest cluster containing the estimates of the highest quality is established. Cluster Φ_6 is the largest cluster which also contains the estimates of highest quality q_{\max} , therefore, the final azimuth is calculated as the weighted mean of the estimates contained in this cluster. Cluster Φ_4 , on the other hand, does not meet the lower bound of allowed cluster size n_{\min} , while cluster Φ_5 is of sufficient size, however, it does not contain estimates of sufficient

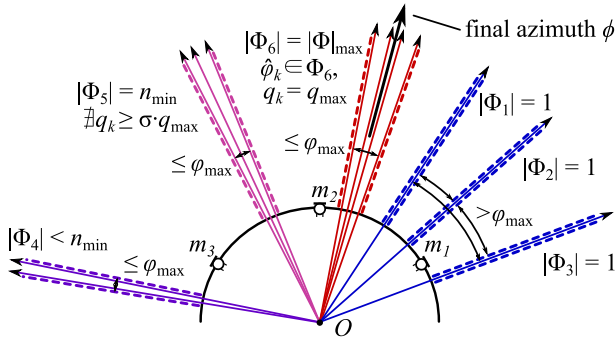


Fig. 8 A graphical example of the partitioning procedure for finding coherent directions among intermediate azimuth estimates and the estimation of the final azimuth estimate according to Algorithm 1

quality. Thus, these two clusters do not meet the criteria of Algorithm 1 and are omitted from analysis.

To determine the increased computational efficiency of our proposed method, we quantify the reduction in the number of cross-correlations required for computing SRP-PHAT and our method, as cross-correlation is the most resource-demanding operation in both methods. SRP-PHAT will calculate $n_h \cdot \binom{M}{2}$ cross-correlations; our method will calculate $\delta \cdot |A|$ cross-correlations, where $\delta = \sum \delta_{ij}$ is the total number of shifts required for calculating cross-correlations for all microphone pairs $(m_i, m_j) \subseteq A$. As the time delay τ is bounded by τ_{max} and τ is expressed in delay in samples Δn , then Δn is also bounded by a maximal sample shift: $\Delta n \in [-\Delta n_{max}, \Delta n_{max}]$, where Δn_{max} is calculated as

$$\Delta n_{max} = \left\lfloor l \cdot \frac{f_s}{c} \right\rfloor, \tag{19}$$

where $\lfloor \cdot \rfloor$ denotes rounding to the largest previous integer (i.e., the floor function). Consequently, cross-correlation $R_{ij}(\Delta n)$ will require $\delta_{ij} = 2\Delta n_{max}(i, j) + 1$ shifts to cover all possible TDOA values. In our experiments we set $M = 6$ and $n_h = 500$ for both UCA prototypes. The number of cross-correlations per each SRP-PHAT computation is then equal to $500 \cdot \binom{6}{2} = 500 \cdot 15 = 7500$. According to (14), in case of $M = 6$ the proposed method utilizes $|A| = 12$ pairs of microphones: 6 consecutive pairs $m_i m_{i+1}$ and 6 pairs over one microphone $m_i m_{i+2}$. Assuming $c = 340$ m/s, for prototype 1 UCA ($r = 7.5$ cm, $f_s = 48$ kS/s) the number of cross-correlations per each DOA evaluation using the proposed method is then equal to $6 \cdot 21 + 6 \cdot 43 = 384$. For prototype 2 UCA ($r = 10$ cm, $f_s = 20$ kS/s) the number of cross-correlations is equal to $6 \cdot 11 + 6 \cdot 23 = 204$. Therefore the number of resource-demanding operations is reduced by more than one order of magnitude.

4.3 Information fusion and shooter localization

As a result of shot detection, the fusion node receives K packets $\{\mathbf{x}, \beta, \mathbf{t}, \Phi\}_k, k = 1, \dots, K$, where K is the number of active UGS, which have detected at least one gunshot event. The number of detected events E_k may vary per UGS. The DOA estimates Φ_k are first steered to the global coordinate system, $\Phi_k \leftarrow \Phi_k - \beta_k$, and information fusion is then conducted in the following steps: identification of SW and MB DOA; estimation of shot geometry; estimation of miss distance and distance to shooter for each UGS; shooter localization.

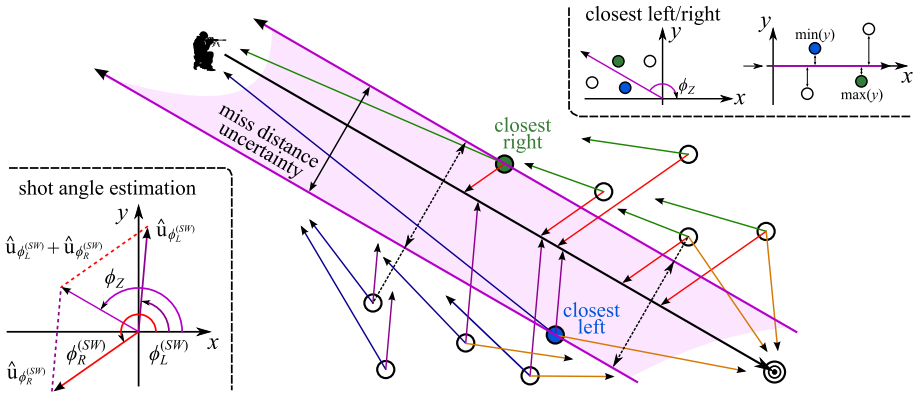


Fig. 9 Shot angle and miss distance uncertainty interval estimation by UGS groups, situated to the left and to the right from the bullet’s trajectory

Information fusion is performed on multiple fusion nodes which can govern a single UGS group or several either intersecting or separate groups. Furthermore, each UGS may be permitted to act as a fusion node if its computational resources allow for it. As a result, several position estimates may be produced for the same shot instance. This paper does not concern the further steps at higher levels of data fusion, where these various estimates are analyzed. This section presents the solution for shooter localization performed on a single fusion node.

4.3.1 DOA coherency

Consistent DOA are established by analyzing all $\Phi = \{\Phi_k \mid k = 1, \dots, K\}$ estimates. To locate coherent estimates, the angular values in Φ are clustered in a manner, similar to the one described in Sect. 4.2.2. If coherent estimates exist, we obtain P clusters $\Phi_p, p = 1, \dots, P$, each containing n_p estimates $\phi_i, i = [1, n_p]$.

Assuming Scenario V (Fig. 2), Φ_p will contain SW DOA corresponding to the detected SW of UGS situated to the left and to the right from the bullet’s trajectory, MB DOA, and other readings, like DOA of TH, various reflections and noise. The DOA of SW vary only slightly (due to DOA estimation error and natural variation of angle θ) and do not depend on the distance to shooter; MB DOA, on the other hand, depend on the distance to shooter and UGS cluster dimensions. If the distance to shooter is significantly larger than the width of the UGS cluster, MB DOA will be roughly parallel for all UGS. At a closer distance the UGS situated on the opposite sides of the bullet’s trajectory will have their MB DOA significantly skewed towards the trajectory in the shooter’s direction. A principle diagram of coherent DOA for Scenario V is presented in Fig. 9.

4.3.2 Event identification and shot geometry estimation

To reduce the error of individual DOA estimates, event identification is performed on the mean values of clusters $\Phi_p: \bar{\phi}_p = \frac{1}{n_p} \sum \Phi_p, p = 1, \dots, P$. To identify SW DOA, all $\bar{\phi}_p$ are analyzed pairwise. For each pair $\bar{\phi}_i, \bar{\phi}_j, i = [1, P - 1], j = [i + 1, P]$, a central angle ϕ_Σ is first calculated as the angular component of the sum of their corresponding unit vectors $\hat{\mathbf{u}}_{\bar{\phi}_i} + \hat{\mathbf{u}}_{\bar{\phi}_j}$ (see Fig. 9). SW DOA are then identified under the assumptions that SW events

are detected first, and at least one SW DOA was detected to the left and to the right from the bullet’s trajectory. Thus $\bar{\phi}_p$ are searched for such $\bar{\phi}_i, \bar{\phi}_j$, that meet all the following conditions:

$$\begin{aligned} \frac{\pi}{2} - \varphi_{\max}^{(SW)} < |\phi_{\Sigma} - \bar{\phi}_i| < \frac{\pi}{2} - \varphi_{\min}^{(SW)}, \\ \frac{\pi}{2} - \varphi_{\max}^{(SW)} < |\phi_{\Sigma} - \bar{\phi}_j| < \frac{\pi}{2} - \varphi_{\min}^{(SW)}, \end{aligned} \tag{20}$$

$$\forall_{\text{tk}} (t_{\phi_k} \mid \phi_k \in \Phi_i) = 1, \forall_{\text{tk}} (t_{\phi_k} \mid \phi_k \in \Phi_j) = 1.$$

We define ind as the operation that determines the index of a specific element in a vector of values. $(\varphi_{\min}^{(SW)}, \varphi_{\max}^{(SW)})$ is the interval of SW propagation angle θ (see Sect. 2) expected values, accounting for variance and measurement error. For example, if $\theta \approx 25^\circ$ and $\pm 5^\circ$ measurement deviation are expected, this interval is set to $(\frac{\pi}{9}, \frac{\pi}{6})$. If the conditions are met, $\bar{\phi}_i, \bar{\phi}_j$ and $\phi_k \in \Phi_i \cup \Phi_j$ are labeled $\bar{\phi}_i^{(SW)}, \bar{\phi}_j^{(SW)}$ and $\phi_k^{(SW)}$, respectively. For $\bar{\phi}_i^{(SW)}, \bar{\phi}_j^{(SW)}$, condition (20) also implies that they were measured on the opposite sides of the bullet’s trajectory. Consequently, we adopt their central angle ϕ_{Σ} as the shot angle ϕ_Z estimate (i.e., the angle, at which the bullet travels towards the UGS cluster; see Fig. 9).

Having estimated ϕ_Z , the UGS S_k that have detected SW are placed either into the “left”, or “right” groups G_L, G_R :

$$\begin{aligned} \phi_k^{(SW)} < \phi_Z &\Rightarrow S_k \in G_L, \\ \phi_k^{(SW)} > \phi_Z &\Rightarrow S_k \in G_R. \end{aligned} \tag{21}$$

To estimate the miss distance, $S_k \in G_L \cup G_R$ closest to the bullet’s trajectory are first located. This is done by steering the S_k coordinates \mathbf{x}_k by ϕ_Z towards the x -axis around the UGS common spatial centroid $\bar{\mathbf{x}} = \frac{1}{K} \sum \mathbf{x}_k$ as

$$\begin{pmatrix} x'_k \\ y'_k \end{pmatrix} = \begin{pmatrix} \bar{x} \\ \bar{y} \end{pmatrix} + \begin{pmatrix} \cos(\phi_Z) & \sin(\phi_Z) \\ -\sin(\phi_Z) & \cos(\phi_Z) \end{pmatrix} \begin{pmatrix} x_k - \bar{x} \\ y_k - \bar{y} \end{pmatrix}. \tag{22}$$

Then, as portrayed in Fig. 9, “closest left” and “closest right” UGS \check{S}_L, \check{S}_R are defined as

$$\begin{aligned} \check{S}_L &= S_i, \quad i = \text{ind min}(y'_k), \quad S_k \in G_L, \\ \check{S}_R &= S_j, \quad j = \text{ind max}(y'_k), \quad S_k \in G_R, \end{aligned} \tag{23}$$

and the distance between them, perpendicular to the shot angle, $\phi_Z - \frac{\pi}{2}$, is referred to as the miss distance uncertainty interval. Inside this interval the exact miss distance cannot yet be estimated at this point. We approximate it at a later stage of shooter localization.

To identify the DOA corresponding to MB events, $\bar{\phi}_p$ are searched for such $\bar{\phi}_i, i = [1, P]$, that meet the following condition:

$$|\phi_Z - \bar{\phi}_i| < \varphi_{\max}^{(MB)}, \quad \bar{\phi}_i \neq \bar{\phi}_i^{(SW)}. \tag{24}$$

During MB DOA identification preference is given to $S_k \in G_L \cup G_R$, because SW detection implies that the bullet has passed the UGS, and thus TH will likely not come from the same direction as MB. This way TH DOA will most certainly be avoided. NOI events caused by different noise, on the other hand, are seldom acquired with consistent DOA by a significant number of UGS, and thus their corresponding clusters Φ_p are significantly smaller and the estimates more dispersed. At this stage they are easily separable from the estimates considered for the MB label. Incidental acoustic sources arising in the FOV can be identified and excluded from analysis by general acoustic monitoring and source tracking techniques, e.g., as in Astapov et al. (2013). As a result of MB DOA identification, $\phi_k \in \Phi_i$ meeting condition (24) are labeled $\phi_k^{(MB)}$.

4.3.3 Distance to shooter estimation and shooter localization

Having identified $\phi_k^{(SW)}$ and $\phi_k^{(MB)}$, $k = 1, \dots, K$, where K is now the number of UGS with both detected events, it is possible to accurately compute the TDOA between MB and SW, Δt_k as

$$\begin{aligned} \Delta t_k &= t_{k,i} - t_{k,j}, \\ i &= \operatorname{ind}_{\Phi_k} \left(\phi_k^{(MB)} \right), \quad j = \operatorname{ind}_{\Phi_k} \left(\phi_k^{(SW)} \right). \end{aligned} \tag{25}$$

Based on Δt_k and the k -th UGS miss distance estimate $\hat{d}_{miss}^{(k)}$, it is possible to assess the distance to shooter from the k -th UGS using a closed form solution, proposed by Sallai et al. (2011):

$$d_{S_k,Z} = \frac{1}{2(c^4 - v^4)} \left(A - 2\sqrt{B} \right), \tag{26}$$

where

$$\begin{aligned} A &= -2v^3 \hat{d}_{miss}^{(k)} \sqrt{v^2 + c^2} - 2\Delta t_k c^3 v^2 + 2c^2 \hat{d}_{miss}^{(k)} v \sqrt{v^2 + c^2} - 2\Delta t_k c v^4, \\ B &= -2c^4 v^4 \left(\hat{d}_{miss}^{(k)} \right)^2 + 2(\Delta t_k)^2 c^6 v^4 \\ &\quad + 2(\Delta t_k)^2 c^4 v^6 - 2c^7 \hat{d}_{miss}^{(k)} \Delta t_k v \sqrt{v^2 + c^2} + c^8 (\Delta t_k)^2 v^2 \\ &\quad + 2c^8 \left(\hat{d}_{miss}^{(k)} \right)^2 + 2v^5 \hat{d}_{miss}^{(k)} \sqrt{v^2 + c^2} \Delta t_k c^3. \end{aligned}$$

Projectile velocity can be empirically estimated by inverting equation (1) as $\hat{v} = c/\sin(\hat{\theta})$ and applying it to $\hat{\theta}$, which is computed as $\hat{\theta} = \bar{\phi}_L^{(SW)} - (\pi - \phi_Z)$, where $\bar{\phi}_L^{(SW)}$ is the mean value of the set of estimates, labeled as SW and belonging to the left group. For $\hat{d}_{miss}^{(k)}$ estimation, a minimal and maximal miss distance interval $[d_{\min}^{(k)}, d_{\max}^{(k)}]$ is first established.

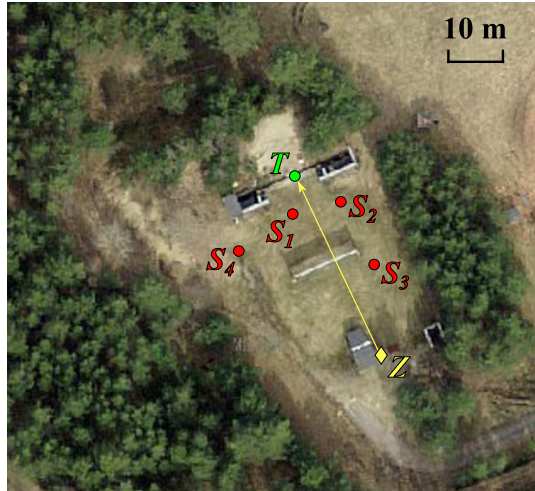
For every S_k , its minimal miss distance $d_{\min}^{(k)}$ spans from its coordinates \mathbf{x}_k in the direction towards the bullet's trajectory (perpendicularly to ϕ_Z) up to the point, where miss distance ambiguity starts; the maximal distance $d_{\max}^{(k)}$ spans further, up to the point, where miss distance ambiguity ends (see dashed line spanning from UGS of the right group in Fig. 9).

Equation (26) suggests that $d_{S_k,Z}$ rises with $\hat{d}_{miss}^{(k)}$, therefore, $S_k \in G_L$ will give larger, and $S_k \in G_R$ —smaller estimates if $\hat{d}_{miss}^{(k)}$ is at the ambiguity start of group G_R , and vice versa if it is at the ambiguity start of G_L . So, the ambiguity interval is iteratively passed from $d_{\min}^{(k)}$ to $d_{\max}^{(k)}$ with a step of d_{step} , the miss distances for K UGS are estimated as $\hat{d}_{miss}^{(k)} = d_{\min}^{(k)} + i \cdot d_{step}$, and distance estimates to shooter $\hat{d}_{S_k,Z}(i)$ at each step are obtained using (26). A shooter position estimate $\hat{Z}_k(i)$ is computed per each UGS, using \mathbf{x}_k , $\phi_k^{(MB)}$ and $\hat{d}_{S_k,Z}(i)$. The fitness of $\hat{Z}_k(i)$ point estimates is measured by their average distance from their common centroid $\bar{Z}(i)$:

$$f_{fit}(i) = \frac{1}{K} \sum_{k=1}^K \left\| \bar{Z}(i) - \hat{Z}_k(i) \right\|. \tag{27}$$

The minimum of the fitness function f_{fit} indicates the miss distance estimates, closest to the actual value, $\hat{d}_{miss}^{(k)} \simeq d_{miss}^{(k)}$, and the final shooter's position estimate is selected as $\hat{Z} = \bar{Z}(i)$, where $i = \arg \min (f_{fit}(i))$.

Fig. 10 Layout of Experiment 1. T —target position; Z —shooter position; S_k —UGS positions



5 Experimental results

The proposed shooter localization approach is tested on real gunshot signals, acquired during three separate live experiments at two different outdoor shooting ranges. Experiment 1 was performed at a small shooting range with the shooter-target distance of 35 m. The shooter took one position for the entire experiment. The signals were acquired by 4 UGS. The layout of Experiment 1 is presented in Fig. 10. Experiments 2 and 3 were performed at a larger shooting range with the shooter-target distance of 100 m (from the central shooting position). The shooter took three firing positions during both experiments. The signals were acquired by 6 UGS. In Experiment 2 the UGS were placed in a tight hexagon-shaped cluster, equidistantly positioned 5 m away from the cluster's center. The layout of Experiment 2 is presented in Fig. 11 (left). In Experiment 3, on the other hand, the UGS were distributed more sparsely. The layout of Experiment 3 is presented in Fig. 11 (right). The firearm used in all three experiments was the Husqvarna 8x57JS rifle with the cartridge muzzle velocity equal to $v_0 = 780$ m/s, thus the shockwave is expected to spread approximately at $\theta \simeq 25.8^\circ$ relative to the bullet's trajectory.

UGS latitude/longitude coordinates were measured using a standalone GPS device (Trimble R8 GNSS) since none of the UGS prototypes have GPS locators on board. For data analysis we convert the GPS coordinates into a local planar coordinate system with the target being set as the zeroth coordinate. The steering angle β_k for each UGS is defined as the heading, measured with a high-precision compass. The presented experimental results are already brought to zero steering and the influence of β_k measurement error is not discussed.

Experiment 1 was conducted at a shooting range surrounded by scattered trees. A bullet-catching sand mound is situated approximately 5 m behind the target. The shooter's position is situated beside a small concrete safety bunker, which obstructed direct line of sight of UGS S_4 . An overhead horizontal barrier is situated in the middle of the shooting range. The shooter fired 30 shots from a standing position; as the target and all UGS were raised by approximately 1 meter from the ground, each bullet passed the cluster at UGS level or slightly higher. Layout coordinates in meters are presented in Table 1. Weather conditions were the following: temperature $t^\circ \simeq 2^\circ\text{C}$, cloudiness 10%, no precipitation, wind speed 1–2 m/s. Parameters for all steps of the localization process are presented in Table 2.

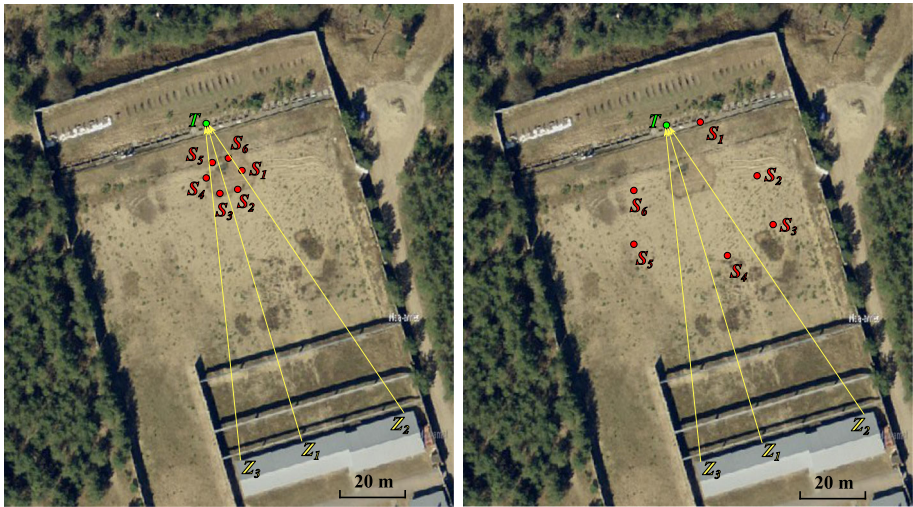


Fig. 11 Layout of Experiments 2 (left) and 3 (right). T –target position; Z_i –shooter positions; S_k –UGS positions

Table 1 Target x_T , firing point x_{Z_i} and UGS x_{S_k} coordinates in meters

Type	Experiment 1	Experiment 2	Experiment 3
x_T	(0, 0)	(0, 0)	(0, 0)
x_{Z_1}	(0, 35)	(0, 100)	(0, 100)
x_{Z_2}	–	(–28.5, 100)	(–28.5, 100)
x_{Z_3}	–	(20, 100)	(20, 100)
x_{S_1}	(4, 6)	(–5, 16)	(–10, 3)
x_{S_2}	(–5.5, 7)	(–2.5, 20.3)	(–20, 20)
x_{S_3}	(–6, 20)	(2.5, 20.3)	(–20, 35)
x_{S_4}	(14, 7.5)	(5, 16)	(–5, 40)
x_{S_5}	–	(2.5, 11.7)	(20, 30)
x_{S_6}	–	(–2.5, 11.7)	(15, 15)

Table 2 Shot detection, DOA estimation and shooter localization parameters

Parameter	Unit	Experiment 1	Experiment 2	Experiment 3
f_s	kS/s	48	20	20
t_W	ms	10	20	20
n_h	–	500	500	500
r_{FOV}	m	0.5	0.5	0.5
σ, n_{\min}	–	0.8, 3	0.8, 3	0.8, 3
$(\varphi_{\min}^{(SW)}, \varphi_{\max}^{(SW)})$	deg.	(21, 31)	(21, 31)	(21, 31)
$\varphi_{\max}^{(MB)}$	deg.	60	40	40
d_{step}	m	0.5	0.5	0.5



Fig. 12 View of the shooting range from the shooter’s position, 100 m away from the target (*top*). UGS placement for Experiment 2 (*bottom*). The span of the bottom image is highlighted on the top image with a red rectangle

Experiment 2 was conducted at a shooting range, which is entirely fenced by tall concrete walls. A bullet-catching sand mound is situated approximately 15–20 m behind the target. The firing points are situated just outside the shooting range hall. Three overhead horizontal barriers are placed along the first 25 m of the range (see Fig. 12 top). The shooter fired 6 shots from each of the three firing points from a standing position. As the target is elevated from the ground level by 3 m, but all UGS were raised by slightly more than 1 meter from the ground, the bullets traveled above the UGS cluster (see Fig. 12 bottom). Layout coordinates in meters are presented in Table 1. Weather conditions were the following: temperature $t^\circ \simeq 8^\circ\text{C}$, cloudiness 50%, no precipitation, wind speed 5–10 m/s. Parameters for all steps of the localization process are presented in Table 2.

Experiment 3 was conducted at the same shooting range as Experiment 2. The same firing points and target position were used. The shooter fired 6 shots from points 1 and 2, and 7 shots from point 3 from a standing position. The UGS are more widely distributed; UGS S_1 is placed at the target’s elevation level, as portrayed in Fig. 13. Layout coordinates in meters are presented in Table 1. Weather conditions were the following: temperature $t^\circ \simeq 6^\circ\text{C}$, cloudiness 100%, light rain, wind speed 9–12 m/s with gusts up to 20 m/s. Parameters for all steps of the localization process are presented in Table 2.



Fig. 13 UGS placement for Experiment 3. Shooting range view is presented in Fig. 12

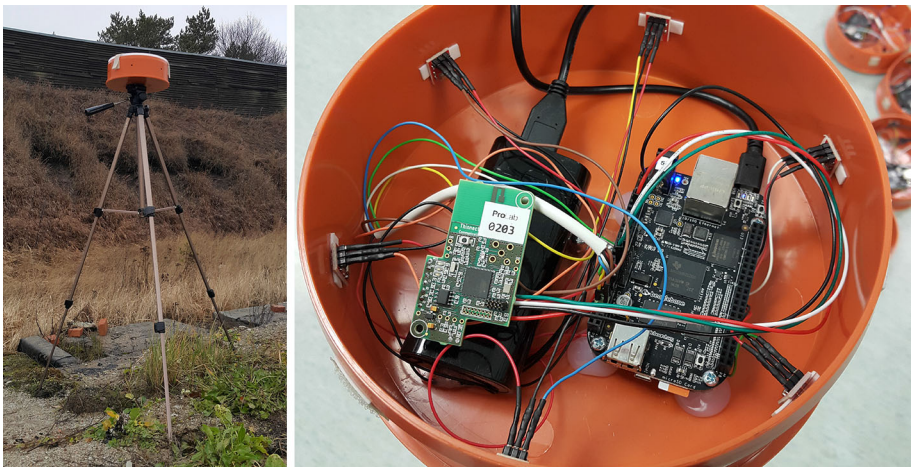


Fig. 14 UGS prototype 2 (*left*). Prototype inner components (*right*)

5.1 Prototype implementation

For the UGS implementation we use Uniform Circular Arrays with $M = 6$ microphones. Two prototypes were created during the course of development. Prototype 1 UGS are used in Experiment 1. Prototype 2 UGS are used in Experiments 2 and 3.

Prototype 1 is composed of a plastic circular shell with the radius of $r = 7.5$ cm, Vansonic PVM-6052 condenser microphones, a multichannel signal amplification circuit and an Agilent U2354A DAQ, connected to a PC running MATLAB. The signals are acquired using the MATLAB Data Acquisition Toolbox at the sampling frequency of $f_s = 48$ kS/s per channel and processed offline. Prototype 1 UGS operate independently from one another, and only rough synchronization is achieved by scheduling the starting moment of data acquisition on each PC. No inter-UGS communication is performed. This cumbersome design is improved upon in prototype 2.

Prototype 2 is composed of an enclosed plastic circular shell with the radius of $r = 10$ cm, ADMP401 MEMS microphones (Pololu Corp., USA), a BeagleBone Black (BBB) development board, a power bank, and a proprietary stand-alone communication module, we call MURP module (see Fig. 14). BBB features two programmable real-time units (PRU) with 32-bit RISC processors, and also an 8-channel 12-bit Analogue Digital Converter (ADC).

This enables the BBB to be used as both a DAQ and processing unit, sampling the data from 6 channels at $f_s = 20$ kS/s separately from the BBB non-real time operating system. The samples produced by PRU are written into a circular memory buffer implemented by the PRUIO library. A circular buffer is used in order to guarantee continuous online signal processing. The binary raw data is also stored on an external SD memory card for later analysis. The sampled data is then fed frame by frame to other software modules, which perform gunshot event detection and DOA estimation. The MURP module (the circuit board found on top of the power bank in Fig. 14) has its own Atmel Atmega256RFR2 chip and IEEE 802.15.4 compliant radio transceiver. A synchronized start time is achieved by broadcasting a sequence of specially timed messages from a control node (six messages counting down from 100 ms with 20 ms intervals), which are used to trigger the concurrent start of signal sampling within the sensor cluster.

The fusion node is implemented on an embedded platform equipped with an Atmel ATmega128RFA1 microcontroller and a IEEE 802.15.4 compliant radio transceiver. In Experiments 2 and 3 the fusion node is used for starting concurrent signal sampling on all the UGS, and no actual data transfer is performed during the experiments, as this paper does not consider the problems of WSN communication. The questions of data validation and network management by a middleware component are discussed in [Preden et al. \(2013\)](#).

5.2 Results of Experiment 1

An example of gunshot event detection by UGS S_3 was presented in Fig. 3. Results show that the applied detection procedure succeeds in detecting gunshot events even with a significantly short TDOA between SW and MB events. During the experiment all 30 shots were detected by all UGS, however, UGS S_4 failed to provide the DOA of seven MB events. Close analysis of signals acquired by UGS S_4 shows that the number of detected events was equal to the number of signal envelope rises per shot. Since the direct line of sight from the shooter to UGS S_4 was obstructed by the safety bunker, the intermediate azimuth estimates did not have sufficient quality to pass the criteria of Algorithm 1 and no final estimates were made. Other UGS detected both SW and MB for every shot; TH was detected in the majority of cases. There were also 13 cases of detection of TH before MB by UGS S_1 and S_2 , the reason being their close position to the target. These results clearly indicate the need of gunshot event identification prior to shooter localization.

The two considered DOA estimation methods succeed in establishing a single distinct direction in the majority of cases. A visualization of DOA estimation intermediate results for UGS S_1 is presented in Fig. 15. SRP-PHAT values for every discrete point are scaled to the maximal value of 0.2; the individual pair-wise estimates of the proposed method are ordered by their cross-correlation peak distinctness from the least to the most sharp and depicted as black, blue, green and red lines, respectively; the thick black line denotes the final estimate. It can be seen that both methods produce one distinct beam and several lesser beams, corresponding to DOA of NOI events. The subplots corresponding to SW detection both show a minor beam in the MB direction. This evidently happens due to short TDOA between the two events and their partial overlapping. The MB itself is very evident in the central pair of subplots. Figure 15 clearly shows that the proposed methods produces results highly similar to the ones of SRP-PHAT.

The DOA estimates of four consecutive shots computed by SRP-PHAT are presented in Fig. 16a, and by the proposed method in Fig. 16b (several estimate values are equal and overlap). It can be seen that SRP-PHAT estimates are more dispersed for UGS S_2 and S_3 . SW, MB and TH events are well distinguishable for both methods, however, results for UGS

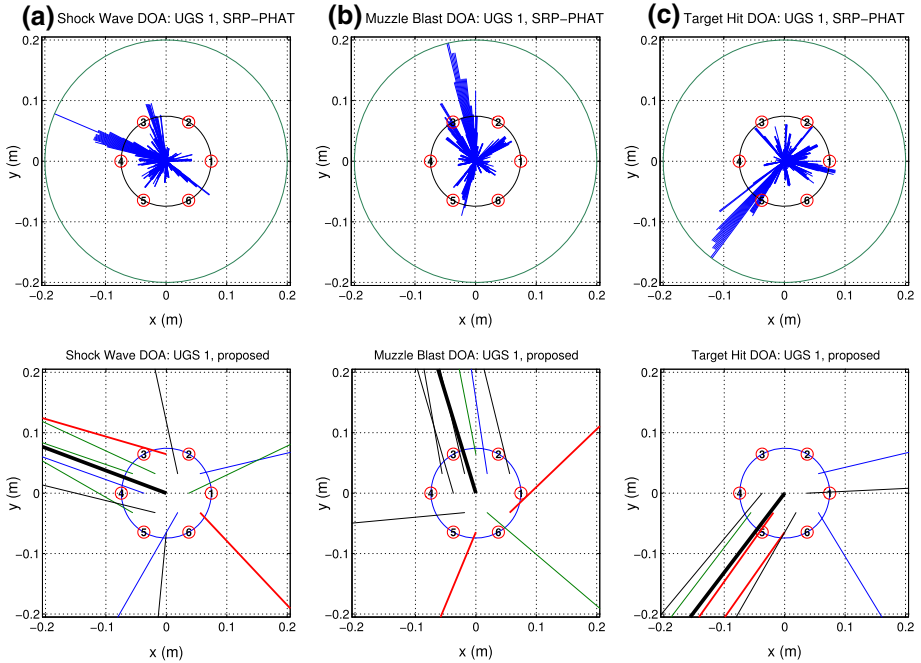


Fig. 15 DOA estimation intermediate results of Experiment 1, UGS S_1 . Top subplots—estimation using SRP-PHAT (blue lines SRP values of points defined in (12), length normalized by the radius of the green circle). Bottom subplots estimation using the proposed method (black, blue, green, red lines estimates of microphone pairs defined in (14), with estimate quality (18) increasing by color, respectively; thick black final estimate)

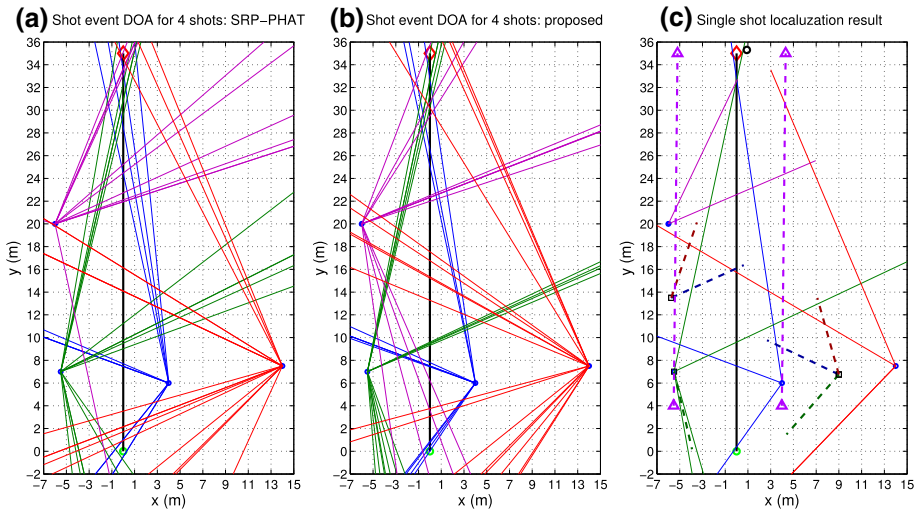


Fig. 16 Experiment 1 DOA estimates for four consecutive shots using **a** SRP-PHAT and **b** the proposed method (red diamond shooter true position; green circle target; blue dots UGS positions; blue, green, purple, red lines DOA estimates of UGS S_1 – S_4 , respectively). **c** Localization result for a single shot (red, blue and green dotted $\hat{\phi}^{(SW)}$, $\hat{\phi}^{(MB)}$ and NOI event DOA of clusters Φ_p ; purple dotted arrow ϕ_Z and miss distance uncertainty; black circle final estimated shooter position)

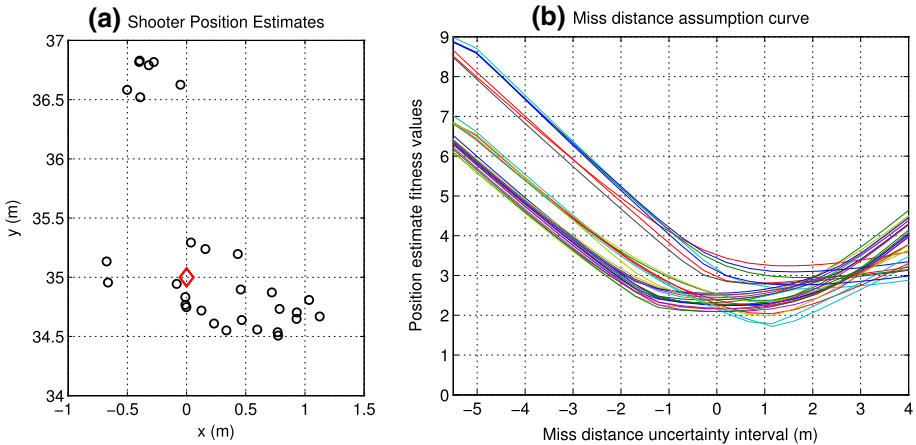


Fig. 17 Experiment 1 results for 30 shots. **a** Estimated shooter positions (*red diamond* shooter true position). **b** Values of f_{fit} , defined in (27), for the miss distance uncertainty interval

Table 3 Shooter position estimate mean error (ME) and standard deviation (SD) in meters

DOA Method	Parameter	Experiment 1	Experiment 2	Experiment 3
SRP-PHAT	\hat{Z} ME	1.12	6.65	8.92
	\hat{Z} SD	0.73	3.53	6.80
Proposed	\hat{Z} ME	0.87	7.08	7.32
	\hat{Z} SD	0.56	3.86	6.15

S_4 are significantly worse due to its larger miss distance and the obstructed line of sight to the shooter.

The intermediate results of localization and the final shooter location estimate for a single shot are presented in Fig. 16c. UGS $\{S_2, S_3\}$ and $\{S_1, S_4\}$, as expected, form clusters of consistent DOA estimates and group into G_L and G_R , respectively. Mean estimates of clustered DOA values are presented in Fig. 16c as dotted lines starting from the spatial centroids of these clusters. The shot angle $\phi_Z \simeq 90^\circ$ is estimated with high accuracy; $\hat{S}_L = S_2$, $\hat{S}_R = S_1$ are correctly assigned, and thus the miss distance uncertainty interval is properly computed.

Final shooter position estimates (using the proposed method for DOA) are presented in Fig. 17a. To quantify the localization accuracy we use the mean error (ME) metric, calculated as the average Euclidean distance between the known and estimated shooter positions:

$$ME = \frac{1}{N_s} \sum_{i=1}^{N_s} \left((x_Z(i) - x_{\hat{Z}}(i))^2 + (y_Z(i) - y_{\hat{Z}}(i))^2 \right)^{1/2}, \quad (28)$$

where N_s is the total number of shots. ME along with its Standard Deviation (SD) for 30 shots is presented in Table 3. It can be seen that using the proposed DOA method results in a slightly smaller ME. Generally, the localization quality for both DOA estimation methods is notably high for Experiment 1. In Fig. 17a a congestion of remote points in the top left corner results from the misdetection of several MB by UGS S_4 . Instantaneous bullet velocity estimation (see Sect. 4.3.3) resulted in $\hat{v} \simeq 740$ m/s, which is consistent with the cartridge

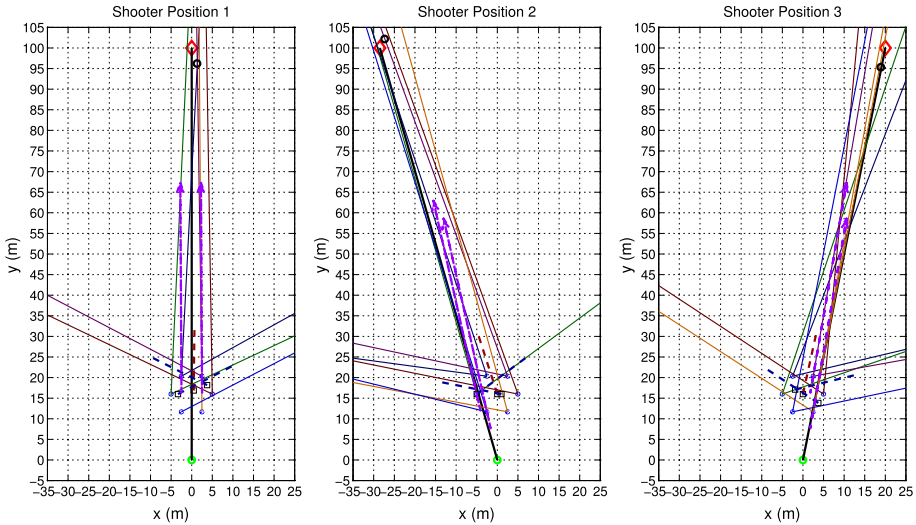


Fig. 18 Experiment 2 localization results for one shot per shooter position (*red and blue dotted*— $\bar{\phi}^{(SW)}$, $\bar{\phi}^{(MB)}$ of clusters Φ_p ; *purple dotted arrow* ϕ_Z and miss distance uncertainty; *black circle* final estimated shooter position)

specification parameters (i.e., velocity of 753 m/s for ranges under 50 m). The values of the fitness function f_{fit} are presented in Fig. 17b. The function’s minimum is situated at ± 1 m from the actual miss distance, and one global minimum of f_{fit} exists for every shot. Thus, miss distance estimation in this case can be performed by a gradient descent method rather than by iterative search.

5.3 Results of Experiment 2

The gunshot acoustic component detection procedure on each UGS succeeded in detecting every shot instance with 5–6 acoustic events per shot on average, occasionally reaching 8–9 events. Acoustic events of Experiment 2 are very similar to the ones of Experiment 3, an example of a single shot signal of which was presented in Fig. 5. The large number of NOI events is caused by numerous reflections of SW, MB, as well as TH off the concrete walls surrounding the shooting range (see Fig. 11). An elevated bullet trajectory, as explained in Section 4.1, causes ground reflections of SW and, consequently, its signal pattern resembles a transient combined with several weaker disturbances. This results in MB being detected as the 3rd or 4th event peak for every shot instance.

The intermediate results of localization and the final shooter location estimate for a single shot case from each of the three firing points are presented in Fig. 18. NOI event DOA are removed from the plots for presentation clarity. For firing point Z_1 all UGS form a single cluster of MB DOA, and UGS $\{S_1, S_2, S_6\}$ and $\{S_3, S_4, S_5\}$ form clusters of SW DOA, detected to the left and right of the bullet’s trajectory and group into G_L and G_R , respectively. For firing points Z_2 and Z_3 MB DOA clusters are also formed from all UGS, because the cluster dimensions are significantly smaller compared to the distance between the cluster and the shooter positions, which results in MB DOA being roughly equal. The clusters of coherent SW DOA estimates are formed for Z_2 from UGS $\{S_1\}$ in the left group and $\{S_2, S_3, S_4, S_5, S_6\}$ —in the right group. For point Z_3 the left group consists of UGS

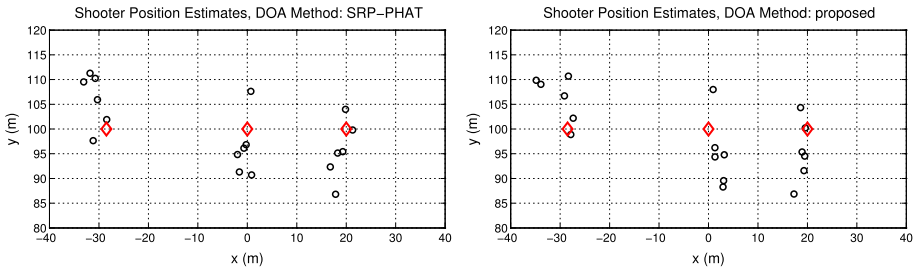


Fig. 19 Experiment 2 localization results for 18 shots with SRP-PHAT (*left*) and the proposed method (*right*) used for DOA estimation. *Black circles* estimated shooter positions; *red diamonds* true shooter positions

$\{S_1, S_2, S_3, S_6\}$ and the right group—of UGS $\{S_4, S_5\}$. As UGS S_1, S_6 and UGS S_3, S_5 are situated nearly along the bullet’s trajectory for points Z_2 and Z_3 , respectively, their belonging to either the left or right group changes from shot to shot. This does not influence the overall localization accuracy, as the considered UGS cluster is dense enough not to drastically change the miss distance ambiguity interval. The shot angles $\phi_{Z_1} \simeq 90^\circ$, $\phi_{Z_2} \simeq 106^\circ$ and $\phi_{Z_3} \simeq 79^\circ$ are estimated with high accuracy.

Final shooter position estimates for all three firing points are presented in Fig. 19. It can be seen that the estimates are significantly more scattered, when compared to the estimates of Experiment 1. Table 3 shows that the ME for Experiment 2 is approximately 7 m, which is notably higher than a ME of approximately 1 m of Experiment 1. However, taking into consideration that the range set for Experiment 2 is almost three times larger, and prototype 2 UGS use an inferior ADC at $f_s = 20$ kS/s, compared to a standalone DAQ of prototype 1 with a larger bit depth and operating at $f_s = 48$ kS/s, the decrease in localization quality is quite expected and justified. Generally, applying both SRP-PHAT and the proposed method of DOA estimation in the localization procedure yields similar localization quality with SRP-PHAT resulting in slightly more accurate estimates.

Bullet velocity estimation resulted in $\hat{v} \simeq 720$ m/s, which is consistent with the cartridge specification parameters (i.e., velocity of 727 m/s for a range of 100 m). Miss distance estimation via the fitness function f_{fit} is less trustworthy for Experiment 2 due to UGS being very closely positioned to each other, which results in very narrow miss distance ambiguity intervals, especially for firing points Z_2 and Z_3 . As a result, if ϕ_Z estimation produces even a slightly inaccurate result, the bullet’s trajectory will not fall into the ambiguity interval and true miss distance estimation fails. In our case ϕ_Z estimation performed accurately enough for the bullet’s trajectory to be at an edge of the ambiguity interval or very close to it, e.g., firing point Z_2 result in Fig. 18. This means that in the minimal value of f_{fit} appears close to the edge of the ambiguity interval. A more spatially distributed UGS cluster would solve this problem.

5.4 Results of Experiment 3

The number of detected gunshot acoustic events is similar to the one of Experiment 2: 5–6 events per shot on average. The situation with reflections off the surrounding walls is worse for UGS S_1, S_2 and S_3 , as they are situated closer to the left and back walls in this case. On the other hand, the effect of SW overlapping with its ground reflection is less evident for the UGS with larger miss distances. Nevertheless, MB is detected as the 3rd peak for 18 out of 19 shot instances.

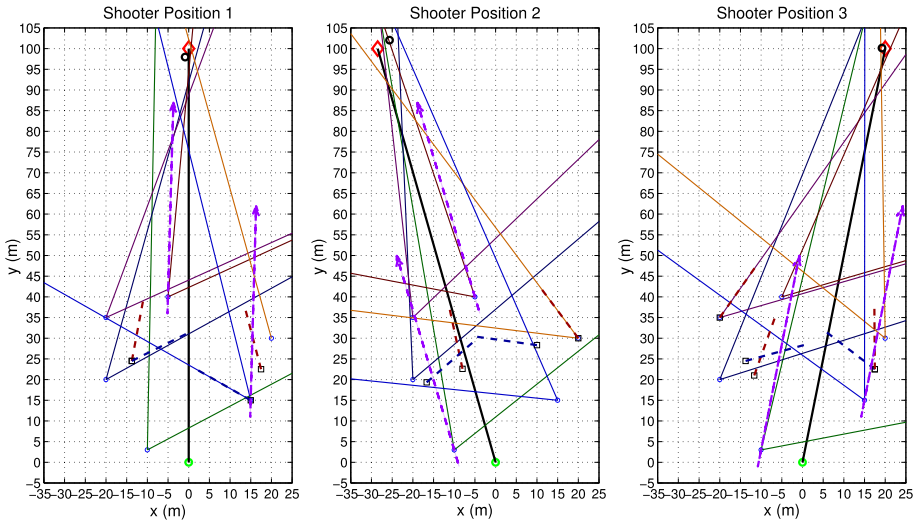


Fig. 20 Experiment 3 localization results for one shot per shooter position ($\bar{\phi}^{(SW)}$, $\bar{\phi}^{(MB)}$ of clusters Φ_p ; purple dotted arrow ϕ_Z and miss distance uncertainty; black circle final estimated shooter position)

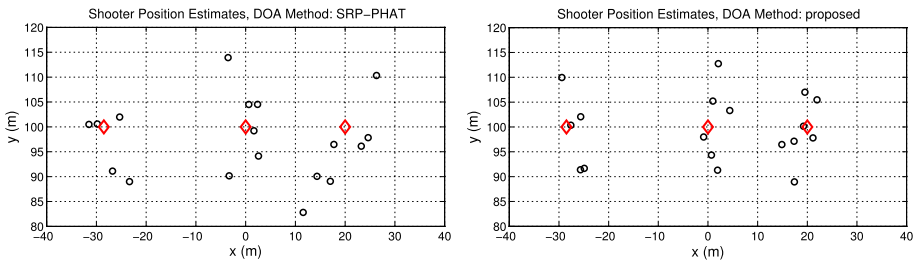


Fig. 21 Experiment 3 localization results for 19 shots with SRP-PHAT (*left*) and the proposed method (*right*) used for DOA estimation. *Black circles* estimated shooter positions; *red diamonds* true shooter positions

The intermediate results of localization and the final shooter location estimate for a single shot from each of the three firing points are presented in Fig. 20. NOI event DOA are removed from the plots for presentation clarity. For point Z_1 UGS $\{S_1, S_2, S_3, S_4\}$ and $\{S_5, S_6\}$ form MB and SW DOA coherent estimate clusters, corresponding to the left and right groups G_L and G_R , respectively. For point Z_2 the UGS belonging to G_L are $\{S_1, S_2, S_3\}$ and belonging to G_R — $\{S_4, S_5, S_6\}$. For point Z_3 the UGS are partitioned as $\{S_1, S_2, S_3, S_4\}$ into G_L and $\{S_5, S_6\}$ —into G_R . As the dimensions of the UGS cluster are large enough to be comparable with the distance from the cluster to the shooter, MB DOA do not form a single coherent direction, as was the case in Experiment 2, rather coherent estimates are formed by UGS situated to the left and right of the bullet’s trajectory and are skewed towards the shooter’s position. Ultimately this can be perceived as a scaled-up version of Experiment 1. The shot angles $\phi_{Z_1} \simeq 90^\circ$, $\phi_{Z_2} \simeq 106^\circ$ and $\phi_{Z_3} \simeq 79^\circ$ are estimated with high accuracy.

Final shooter position estimates for all three firing points are presented in Fig. 21. The estimates are also significantly more scattered, compared to the estimates of Experiment 1. Table 3 presents the ME of localization, calculated using (28). The ME for both Experiments

2 and 3 using the proposed method for DOA estimation is approximately 7 m. The ME of Experiment 3 with SRP-PHAT used as a DOA method is larger, which indicates the supremacy of the proposed method over SRP-PHAT in this case. It can be also noticed from Fig. 21 that Z_2 has only 5 estimates around its true position. This is due to one shot being localized incorrectly and the point residing outside of the figure bounds for both DOA methods. This is a single example of gunshot event identification failure by DOA. If a NOI event has a DOA resembling that of MB and satisfies all the temporal and spatial bounds of the MB check, it can be falsely labeled as MB. Consequently, the TDOA Δt is computed incorrectly and the whole localization procedure can fail. However, this requires the NOI event to corrupt the DOA estimates of several UGS, which is highly unlikely. In our case UGS S_2 and S_3 mistook a NOI event for MB, and their incorrect estimates of distance to shooter steered the cluster's global estimate farther from shooter's true position.

Bullet velocity estimation resulted in $\hat{v} \simeq 725$ m/s, which closely corresponds to the result of Experiment 2. Miss distance estimation via the fitness function f_{fit} operates well for this experiment, as the miss distances for all UGS are sufficient and f_{fit} forms curves, similar to the ones portrayed in Fig. 17, with a single global minimum for the majority of shot instances.

6 Discussion and future work

Although the proposed method of gunshot acoustic component identification using DOA information increases shooter localization robustness, accounting for the destructive influence of various types of NOI events, it has several shortcomings that yet require attention.

The instantaneous bullet velocity estimation via the shot angle needs to be developed into a more general procedure that also accounts for the decrease in bullet velocity with traveled distance. In the experiments the bullet velocity was approximately estimated to be 720–725 m/s, which is significantly less than the 780 m/s muzzle velocity claimed in the cartridge specification. Such velocity reduction even for a 100 m range case can influence localization results. Thus, the degree of this influence needs to be quantified and accounted for in the future.

Alternatively to estimating the distance to shooter by applying (26) in the miss distance ambiguity interval, bearing-only localization methods can be applied. Having identified MB DOA, a least square optimization method, e.g., the bearing-only Total Least Square localization proposed by Dogancay (2005), may be used to estimate the shooter position. However, convergence on the position is doubtful for a tight cluster configuration, like the one used in Experiment 2. Further testing is required to assess the applicability of bearing-only methods under different sensor placement and shooter distance conditions.

The event identification and shooter localization approach needs to be tested in a burst-mode shooting scenario, the peculiarities of which were reviewed in Sect. 4.1. In such a scenario shot instance separation will likely pose a serious problem, so the acoustic event detection procedure will have to be developed further to account for extremely closely spaced shot instances. Also the procedure of sending the shot information to the fusion node is to be reviewed for this case, as sending a large number of packets through the WSN in a very short period of time tends to be problematic.

The problems situated with burst-mode gunshot localization are also related to a case of simultaneous gunshots. If several shots are fired from significantly different shooter positions, the proposed approach in its current state can distinguish between various SW and MB events and produce several position estimates if these gunshot events are not masked by each other and the associated NOI events. The information fusion procedure, however, has to be

complemented with additional conditions, which distinguish between several simultaneous SW events in order to assure that the SW events following the one which is detected first are not treated as NOI events.

We also intend to identify the boundaries of application of the gunshot planar geometry model, where either the shooter's or target's elevation above the UGS cluster starts to influence localization accuracy. If the bullet's trajectory does not lie in the same plane as the UGS cluster, the shot geometry cannot be estimated by a planar model, since the conical wavefront of SW cannot be modeled as a planar wavefront, and distance to shooter cannot be estimated by the horizontal projection of the bullet's trajectory. As the results of Experiment 2 have shown, slight elevation of the target does not influence the localization procedure, however, larger elevation levels were not considered in the experiments.

The main problem situated with UGS implementation is situated with the limitations of signal acquisition and processing in real-time. The results of Experiments 2 and 3 show that the reduction of the sampling rate reduces DOA estimation quality and the overall localization accuracy. The influence of applying reduced sampling rates on DOA estimation quality was discussed by us in [Astapov et al. \(2015b\)](#). Therefore, a hardware configuration with a more powerful ADC needs to be developed for future prototypes in order to assure stable sampling at rates equal or higher than the one used in Experiment 1.

Long-term development plans include the expansion of the localization procedure in order to cover all the possible shot scenarios, which were examined in Sect. 3. The specifics of the remaining scenarios are to be researched and a procedure for distinction between the scenarios is to be developed.

7 Conclusion

The paper discussed the absolute need to distinguish SW and MB gunshot events in a scenario with presence of NOI acoustic events, where the MB transient is not guaranteed to strictly follow the SW transient. A shooter localization procedure comprising gunshot acoustic event identification based on DOA information, gunshot geometry estimation and shooter position estimation was presented and verified on real-life data. The main advantages of the proposed localization procedure include its ability to operate asynchronously in a size-invariant WSN, low dependency on gunshot parameter assumptions and increased noise tolerance.

The proposed gunshot acoustic event identification procedure based on DOA information was shown to successfully distinguish the SW and MB gunshot acoustic components from various NOI events. The proposed DOA estimation method was proven to provide DOA estimates, not inferior to the ones produced by one of the most effective DOA estimation methods of SRP-PHAT, while being more computationally effective. The ability of the proposed localization procedure to estimate the shooter's position at a short and medium range with different sensor cluster configurations and under various weather conditions was demonstrated. The proposed localization procedure exhibits high robustness and tolerance to the destructive influence of acoustic NOI events.

Appendix

Multilateration is a technique of estimating object position coordinates based on TDOA information. For the application of shooter localization in the WSN of ground sensors, the shooter's position can be estimated using the TDOA between the MB events, detected by

different UGS. As the inter-UGS event time values are used, sufficient node synchronization and temporal, as well as spatial data validation are essential for successful operation of multilateration. Furthermore, the method is applicable only if the MB acoustic events are explicitly identified among other detected gunshot events.

The distance between UGS network node k with coordinates (x_k, y_k, z_k) and the shooter can be defined as a vector length

$$d = \sqrt{(x_k - x)^2 + (y_k - y)^2 + (z_k - z)^2}, \tag{29}$$

where (x, y, z) are the shooter’s coordinates and $k = 1, \dots, K$, where K is the total number of UGS. Thus, knowing UGS positions and times of MB event occurrence t_{MB} for a detected gunshot, the TDOA $\tau_{A,B}$ can be found between two separate UGS A and B . The distance difference between UGS A and the shooter and UGS B and the shooter, $d_{A,B}$ is then calculated as

$$\begin{aligned} d_{A,B} &= c \cdot \tau_{A,B} = c(t_{MB}(A) - t_{MB}(B)) \\ &= \sqrt{(x_A - x)^2 + (y_A - y)^2 + (z_A - z)^2} \\ &\quad - \sqrt{(x_B - x)^2 + (y_B - y)^2 + (z_B - z)^2}, \end{aligned} \tag{30}$$

where (x, y, z) are shooter (MB source) coordinates and (x_A, y_A, z_A) are the coordinates of UGS A , and (x_B, y_B, z_B) are the coordinates of UGS B (Liu and Yang 2010). For any group consisting of G UGS the shooter is localizable by the following system of $G - 1$ nonlinear equations:

$$\begin{cases} d_{1,2} = \sqrt{(x_1 - x)^2 + (y_1 - y)^2 + (z_1 - z)^2} - \sqrt{(x_2 - x)^2 + (y_2 - y)^2 + (z_2 - z)^2} \\ d_{1,3} = \sqrt{(x_1 - x)^2 + (y_1 - y)^2 + (z_1 - z)^2} - \sqrt{(x_3 - x)^2 + (y_3 - y)^2 + (z_3 - z)^2} \\ \dots \\ d_{1,G} = \sqrt{(x_1 - x)^2 + (y_1 - y)^2 + (z_1 - z)^2} - \sqrt{(x_G - x)^2 + (y_G - y)^2 + (z_G - z)^2} \end{cases},$$

where $d_{i,j}$ is the distance difference between the i -th and j -th UGS, and $G \leq K$ is the number of UGS in the group. To estimate the solution to this system of nonlinear equations at least four UGS that have detected MB are needed; this yields three TDOA values $\tau_{1,2}, \tau_{1,3}, \tau_{1,4}$, and the system is solved by applying a least squares method, e.g., Levenberg-Marquardt. Various practical approaches exist, e.g., as discussed by Bancroft (1985) or by Bucher and Misra (2002). For the ground applications we could simplify the solution with constant z dimension and denote the unknown location of the shooter as (x, y) ; then we can use the t_{MB} values from only three UGS.

Multilateration methods for WSN highly depend on inter-node synchronization accuracy. Figure 22 presents the results of a simulation of shooter localization using multilateration for the setup identical to that of Experiment 3 (see Sect. 5). The figure illustrates the localization accuracy for all $\binom{6}{4} = 15$ combinations of $G = 4$ UGS groups and $\binom{6}{6} = 1$ combination of $G = 6$ UGS groups with the synchronization error of each UGS randomly chosen from a uniform distribution within the interval of ± 10 ms. The figure shows that larger UGS groups perform with better accuracy than smaller groups with the same degree of node synchronization error. To illustrate the impact of WSN synchronization error on shooter localization accuracy, shooter position estimate mean error (ME), calculated by (28), and its standard deviation (SD) are presented for $G = 4$ and $G = 6$ UGS groups in Table 4. For this simulation we also use the setup of Experiment 3 and assume the WSN clock synchronization error to be in a range of ± 5 ms and up to ± 50 ms. The table shows that in

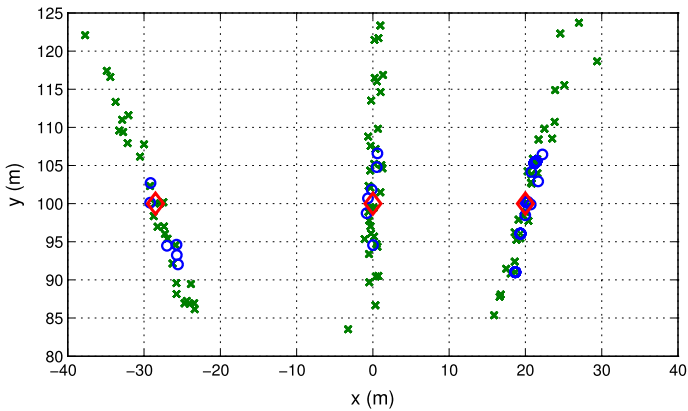


Fig. 22 Shooter localization simulation results for Experiment 3 using multilateration. The theoretical node clock synchronization error is uniformly distributed within the interval of ± 10 ms. *Blue circles* shooter positions estimated with $G = 6$ UGS groups; *green crosses* shooter positions estimated with $G = 4$ UGS groups; *red diamonds* true shooter positions

Table 4 Shooter position estimate mean error (ME) and standard deviation (SD) in meters

Node Synchron. Error	Parameter	UGS group $G = 4$	UGS group $G = 6$
± 5 ms	\hat{Z} ME	6.79	2.57
	\hat{Z} SD	8.43	1.87
± 10 ms	\hat{Z} ME	11.29	5.21
	\hat{Z} SD	12.88	3.92
± 20 ms	\hat{Z} ME	16.79	11.88
	\hat{Z} SD	17.35	10.01
± 50 ms	\hat{Z} ME	23.09	22.45
	\hat{Z} SD	24.20	22.61

order to obtain shooter position estimate accuracy comparable to our proposed method, the $G = 6$ UGS groups should be synchronized to at least ± 10 ms, and for $G = 4$ UGS groups the synchronization should be within ± 5 ms.

References

- Aguilar, J. (2013). Gunshot location systems the transfer of the sniper detection technology from military to civilian applications. In: Proceedings of 47th international carnahan conference on security technology (ICCST), pp 1–6
- Aguilar, J. R., Salinas, R. A., & Abidi, M. A. (2007). Acoustical model of small calibre ballistic shock waves in air for automatic sniper localization applications. Proceedings of SPIE 6538, sensors, and command, control, communications, and intelligence (C3I) technologies for homeland security and homeland defense VI 6538:65,381D–65,381D–8
- Ash, J., Whipps, G., & Kozick, R. (2010). Performance of shockwave-based shooter localization under model misspecification. In: Proceedings of 2010 IEEE international conference on acoustics speech and signal processing (ICASSP), pp 2694–2697

- Astapov, S., Berdnikova, J., & Preden, J. S. (2013). Optimized acoustic localization with SRP-PHAT for monitoring in distributed sensor networks. *International Journal of Electronics and Telecommunications*, 59(4), 383–390.
- Astapov, S., Berdnikova, J., & Preden, J. S. (2015a). A two-stage approach to 2D DOA estimation for a compact circular microphone array. In: Proceedings of 4th international conference on informatics, electronics and vision (ICIEV), pp 1–6
- Astapov, S., Ehalá, J., & Preden, J. S. (2015b). Performing acoustic localization in a network of embedded smart sensors. *International Journal of Microelectronics and Computer Science (IJMCS)*, 6(3), 86–95.
- Bancroft, S. (1985). An algebraic solution of the gps equations. *IEEE Transactions on Aerospace and Electronic Systems AES*, 21(1), 56–59.
- Borzino, A., Apolinario, J., & de Campos, M. (2014). Estimating direction of arrival of long range gunshot signals. In: Proceedings of international telecommunications symposium (ITS), pp 1–5
- Bucher, R., & Misra, D. (2002). A synthesizable VHDL model of the exact solution for three-dimensional hyperbolic positioning system. *VLSI Design*, 15(2), 507–520.
- Carlucci, D., & Jacobson, S. (2010). *Ballistics: Theory and design of guns and ammunition*. Boca Raton: Taylor & Francis.
- Damarla, T., Kaplan, L., & Whipps, G. (2010). Sniper localization using acoustic asynchronous sensors. *IEEE Sensors Journal*, 10(9), 1469–1478.
- DiBiase, J. (2000). A high-accuracy, low-latency technique for talker localization in reverberant environments using microphone arrays. PhD thesis, Brown University, Providence, RI, USA
- Dogancay, K. (2005). Bearings-only target localization using total least squares. *Signal Processing*, 85(9), 1695–1710.
- Freire, I., & Apolinario, J. (2011). GCC-based DoA estimation of overlapping muzzleblast and shockwave components of gunshot signals. In: Proceedings of IEEE second Latin American symposium on circuits and systems (LASCAS), pp 1–4
- George, J., & Kaplan, L. (2011). Shooter localization using soldier-worn gunfire detection systems. In: Proceedings of 14th international conference on information fusion (FUSION), pp 1–8
- George, J., Kaplan, L., Deligeorges, S., & Cakiades, G. (2014). Multi-shooter localization using finite point process. In: Proceedings of 17th international conference on information fusion (FUSION), pp 1–7
- Libal, U., & Spyra, K. (2014). Wavelet based shock wave and muzzle blast classification for different supersonic projectiles. *Expert Systems with Applications*, 41(11), 5097–5104.
- Lindgren, D., Wilsson, O., Gustafsson, F., & Habberstad, H. (2009). Shooter localization in wireless sensor networks. In: Proceedings of 12th international conference on information fusion (FUSION), pp 404–411
- Liu, Y., & Yang, Z. (2010). *Location, localization, and localizability: Location-awareness technology for wireless networks*. New York: Springer Science & Business Media.
- Mazurek, J. A., Barger, J. E., Brinn, M., Mullen, R. J., Price, D., Ritter, S. E., & Schmitt, D. (2005). Boomerang mobile counter shooter detection system. In: Proceedings of SPIE 5778, sensors, and command, control, communications, and intelligence (C3I) Technologies for Homeland Security and Homeland Defense IV, vol 5778, pp 264–282
- Millet, J., & Baligand, B. (2006). *Latest achievements in gunfire detection systems*. Tech. rep. DTIC Document
- Osborne, R., Bar-Shalom, Y., George, J., & Kaplan, L. (2014). Data fusion from multiple passive sensors for multiple shooter localization via assignment. In: Proceedings of 17th international conference on information fusion (FUSION), pp 1–7
- Preden, J. S., Llinas, J., Rogova, G., Pahtma, R., & Motus, L. (2013). On-line data validation in distributed data fusion. *SPIE defense, security and sensing, ground/air multisensor interoperability, integration, and networking for persistent ISR IV, International Society for Optics and Photonics*, 8742, 1–12.
- Sallai, J., Volgyesi, P., Pence, K., & Ledeczki, A. (2011). Fusing distributed muzzle blast and shockwave detections. In: Proceedings of 14th international conference on information fusion (FUSION), pp 1–8
- Sallai, J., Volgyesi, P., Ledeczki, A., Pence, K., Bapty, T., Neema, S., & Davis, J. (2013). Acoustic shockwave-based bearing estimation. In: Proceedings of ACM/IEEE International conference on information processing in sensor networks (IPSN), pp 217–228



Sergei Astapov received his Ph.D. degree in the field of Computer System Engineering at the Tallinn University of Technology in 2016. He continues his research at the Department of Software Science at the Tallinn University of Technology and is a member of the Department's Research Laboratory for Proactive Technologies. His research interests include object localization and tracking using wide-band signal analysis, data mining and classification tasks, as well as distributed computing and data fusion algorithms for situation awareness in cyber-physical systems. His recent research concerns object localization and event identification in open environments and acoustic signal based diagnostics of industrial machinery.



Julia Berdnikova received her M.Sc. degree in Telecommunication at the Tallinn University of Technology in 2003. She works as a research scientist and continues her education as a Ph.D. student at the Thomas Johann Seebeck Department of Electronics at the Tallinn University of Technology. Her research interests include digital signal processing, radar and sonar engineering, object classification tasks and distributed sensor networks.



Johannes Ehala received his M.Sc. degree in the field of Computer System Engineering at the Tallinn University of Technology in 2012. Currently he is a Ph.D. student at the Department of Software Science at the Tallinn University of Technology and is a member of the Research Laboratory for Proactive Technologies. His doctoral studies and research interests include self-organization and emergent behavior in cyber-physical-social systems and computational models of distributed computer systems. Currently he is involved in analyzing the temporal aspects of interactions and their implications on the semantic interpretation of interactions in distributed computer systems.



Jaanus Kaugerand received his M.Sc. degree in the field of Computer System Engineering at the Tallinn University of Technology in 2014. Currently he is a Ph.D. student at the Department of Software Science at the Tallinn University of Technology and is a member of the Research Laboratory for Proactive Technologies. His doctoral studies and research interests include dependability in proactive distributed networked systems and emergent behavior. Currently he is involved in analyzing the temporal aspects of interactions and their implications on the semantic interpretation of interactions in distributed computer systems.



Jürjo-Sören Preden received his Ph.D. degree in Computer Science from the Tallinn University of Technology. He is a senior researcher and the head of the Research Laboratory for Proactive Technologies at the Tallinn University of Technology. Jürjo's research interests are focused on distributed computing systems, more specifically on cognition and situation awareness of such systems. His spectrum of activities involves sensing technologies, data processing, computation and communication in ad-hoc sensing systems. Jürjo represents Estonia in NATO STO SCI panel as a national representative.